



THE UNIVERSITY OF
WAIKATO
Te Whare Wānanga o Waikato

Research Commons

<http://waikato.researchgateway.ac.nz/>

Research Commons at the University of Waikato

Copyright Statement:

The digital copy of this thesis is protected by the Copyright Act 1994 (New Zealand).

The thesis may be consulted by you, provided you comply with the provisions of the Act and the following conditions of use:

- Any use you make of these documents or images must be for research or private study purposes only, and you may not make them available to any other person.
- Authors control the copyright of their thesis. You will recognise the author's right to be identified as the author of the thesis, and due acknowledgement will be made to the author where appropriate.
- You will obtain the author's permission before publishing any material from the thesis.

Studies Towards a pH-Sensitive Anticancer Prodrug Model



THE UNIVERSITY OF
WAIKATO
Te Whare Wānanga o Waikato

A thesis submitted in partial fulfilment of the
requirements for the degree of
Master of Science in Chemistry

at

The University of Waikato

by

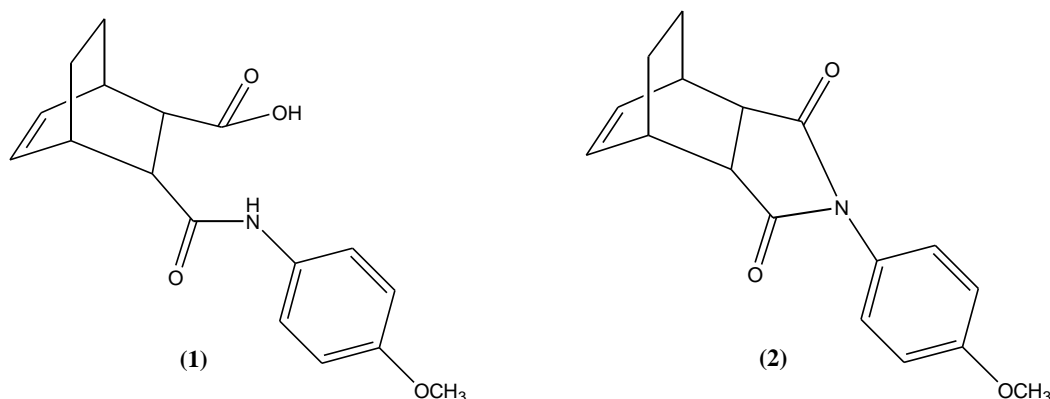
Xiao Shi Teng

The University of Waikato

2010

Abstract

Tumour-activated prodrug (TAP) is designed to aim at increasing the prodrug selectivity to kill cancer cells. One strategy to is to design a TAP containing an amine cytotoxin, present as an amide function, which could be released more rapidly in the low pH environment of tumour tissues when amide undergoes hydrolysis.



The prodrug model **(1)** was the subject of the current study. At lower pH its un-ionised carboxylic acid group provides neighbouring catalysis of hydrolysis of the adjacent amide. It was synthesised via ring-opening of the imide **(2)** which itself was directly synthesised from *endo*-bicyclo[2.2.2]octa-5-ene-2,3-dicarboxylic anhydride and *p*-methoxyaniline.

The pH-rate profile of **(1)** was established over the pH range of 3-10, covering rapid hydrolysis of un-ionised acid-amide at lower pH but slower imide formation above pH 8 from the ionised acid-amide. From the kinetic data were calculated the dissociation constant for **(1)** (pK_a : 5.1 at 30°C) and limiting lower pH rate constant for hydrolysis of **(1)** in its fully neutral form (k_{lim} : 0.44 min^{-1} at 30°C). The data in the pH range of 8-10 provided k_{low} (0.067 min^{-1}) representing formation of **(2)** from fully ionised **(1)**.

The following equilibrium reaction was also investigated at high pH, at which **(1)** was in its fully ionised amide carboxylate form, by kinetic studies on **(2)** in hydroxide solutions.



The second order rate constant for the forward reaction, k_f , was $74 \text{ L mol}^{-1} \text{ min}^{-1}$ which with k_{low} for the reverse reaction gave K as 1100 L mol^{-1} .

Acknowledgements

First and foremost, I would like to thank my supervisor Associate Professor Lyndsay Main who provided me the opportunity to work with the anticancer prodrug project which I enjoyed very much. Thanks for your guidance and patience in directing the research and reading the thesis. I could never have done it without you!

I would also like to thank everyone in the Chemistry Department for your friendliness and technical support. In particular, Pat Gread (IR and equipment lender), Wendy Jackson (SOP trainings), Jolene Brown and Ben Deadman (NMR). A big thanks too to everyone in lab E.3.14 who kept me accompanied for the past two years and supported me with all the help I needed.

A special thanks to Dr. Neville Strick who took care of my knee surgery so well that I did not have to worry about postponing my degree while I was lying on the hospital bed.

I am heartily thankful for all my dear friends who have always been there for me, especially when I need someone to chat to, or just to share a coffee with. A special thanks also needs to go out to Uncle David Deng, Uncle John Wu and Vivian Lang who were so kind to proof-read my thesis at the very last minute.

Last but not least, I would like to thank my family for their love and support (both morally and financially) all these years; I could never have come this far without all of you.

Table of Contents

Abstract.....	ii
Acknowledgements.....	iv
Table of Contents.....	v
List of Figures	vii
List of Tables	viii
List of Abbreviations	ix
1 Introduction	1
1.1 Cancer	1
1.1.1 What is cancer?.....	1
1.1.2 Types of Cancer.....	5
1.1.3 Treatments targeting cancer cells.....	5
1.2 Tumour-Activated Prodrug	6
1.2.1 Disadvantages of most anticancer drugs today.....	6
1.2.2 Prodrugs.....	7
1.2.3 Tumour-activated prodrugs.....	7
1.2.4 pH-sensitive TAPs.....	8
1.3 Amide Hydrolysis	12
1.3.1 Glüsenkamp's Investigations	13
1.4 Previous work.....	16
1.5 Project Aim.....	19
2 Results and Discussions	20
2.1 Preparation of endo-bicyclo[2.2.2]octa-5-ene-2,3-dicarboxylic anhydride 3 ..	20
2.2 Attempted syntheses of acid-amide using N-methylaniline.....	22
2.2.1 Introduction	22
2.2.2 Attempted synthesis of amide ester 8.....	24
2.2.3 Direct synthesis of acid-amide 7	25
2.3 Attempted synthesis of acid-amide using p-methoxyaniline	25
2.3.1 Introduction	25
2.3.2 Synthesis of acid-amide 9	25
2.3.3 Synthesis of imide 10	27
2.4 Kinetic Studies of reversible ring-opening of imide 10.....	29
2.4.1 Rate constants for forward and reverse reactions	29

2.4.2	Equilibrium Constant, K.....	31
2.5	Kinetic studies towards acid-amide 9 using buffer solutions	33
2.5.1	Introduction	33
2.5.2	pH rate profile of ionised acid-amide	35
2.5.3	pH rate profile incorporating neutral acid-amide.....	37
3	Materials and Methods.....	43
3.1	Materials	43
3.2	General methods	43
3.3	Preparation of compounds	44
3.3.1	<i>endo</i> -Bicyclo[2.2.2]octa-5-ene-2,3-dicarboxylic anhydride 3	44
3.3.2	Attempted synthesis of amide ester 7	45
3.3.3	Attempted direct synthesis of acid-amide 7	47
3.3.4	Attempted synthesis of acid-amide 9	47
3.3.5	Synthesis of imide 10	48
3.4	Solutions preparation for kinetic studies of ring-opening of imide 10.....	49
3.4.1	Calculation of rate constants for forward and reverse reactions (k_f and k_r) 50	
3.5	Kinetic studies of acid-amide 9 conversion using various buffer solutions.....	51
3.5.1	Introduction	51
3.5.2	Preparation of buffer solutions.....	52
3.5.3	Kinetic studies to establish pH-rate profile of acid-amide 9.....	54
3.5.4	Buffer dilutions.....	55
4	Summary and Conclusions	57
	References	60
	Appendix A – Glycolytic pathway.....	65
	Appendix B – ^1H NMR spectrum of imide 10	66
	Appendix C – Graph for determining errors	67
	Appendix D – Error estimation of k_{lim} and pK_a	69
	Appendix E – UV/Vis spectra obtained from Agilent Chemstation Software	72
	Appendix F – Theory of first order rate constants ³²	74

List of Figures

FIGURE 1-1: FORMATION OF CANCEROUS CELL BY EXPOSURE TO CARCINOGENS	2
FIGURE 1-2: GENERAL LAYOUT OF A TUMOUR-ACTIVATED PRODRUG (TAP) DESIGN	8
FIGURE 1-3: MENGER'S PEPTIDASE MODEL	12
FIGURE 1-4: HYDROLYSIS OF <i>N</i> -METHYLPHTHALAMIC ACID	13
FIGURE 1-5: GLÜSENKAMP'S BICYCLIC ANHYDRIDES (A, LEFT) AND THEIR CORRESPONDING <i>N</i> - METHYLTRYPTAMINE DERIVATIVES (B, RIGHT) AS MODEL AMIDES	14
FIGURE 1-6: GLÜSENKAMP'S ACID AMIDE 9B - HIGH HYDROLYSIS RATE	15
FIGURE 1-7: SYNTHETIC ROUTE TO ACID-AMIDE	17
FIGURE 1-8: CYCLISATION OF ACID-AMIDE TO RELEASE AMINE	17
FIGURE 1-9: PH-RATE PROFILE OF ACID-AMIDE	18
FIGURE 2-1: SYNTHESIS OF <i>ENDO</i> -BICYCLO[2.2.2]OCTA-5-ENE-2,3-DICARBOXYLIC ANHYDRIDE	20
FIGURE 2-2: DEFINITION OF <i>ENDO</i> AND <i>EXO</i> SUBSTITUENT	20
FIGURE 2-3: FORMATION OF THE <i>ENDO</i> -PRODUCT VIA DIELS-ALDER CYCLOADDITION REACTION	21
FIGURE 2-4: SYNTHESIS ROUTE TO ACID-AMIDE 7	22
FIGURE 2-5: ESTERIFICATION OF ACID-AMIDE SALT 6	23
FIGURE 2-6: FORMATION OF IMIDE DUE TO USE OF A PRIMARY AMINE	24
FIGURE 2-7: A DIRECT SYNTHESIS OF ACID-AMIDE 7 FROM <i>ENDO</i> -ANHYDRIDE 3	24
FIGURE 2-8: SYNTHESIS OF ACID-AMIDE 9	26
FIGURE 2-9: SYNTHESIS OF IMIDE 10	27
FIGURE 2-10: CONVERSION OF IMIDE TO CORRESPONDING ACID-AMIDE 9	28
FIGURE 2-11: GRAPH OF K_{OBS} AGAINST $[OH^-]$	30
FIGURE 2-12: AN EXAMPLE OF THE UV/VIS REPETITIVE SCANNING SPECTRUM OF 1:1 CARBONATE BUFFER (PH 9.43)	36
FIGURE 2-13: IMIDE RING-OPENING EQUILIBRIUM REACTION STUDIED BY SHAFER <i>ET AL.</i> ²³	37
FIGURE 2-14: PH RATE PROFILE ESTABLISHED FOR ACID-AMIDE 9 [30.0°C, μ 1.00 (KCL)]. THE BEST FIT LINE IS BASED ON EQUATION (7) (SEE LATER).	38
FIGURE 2-15: GRAPH OF $1/(K_{OBS}-K_{LOW})$ VS $1/[H^+]$	41
FIGURE 2-16: KLUGER'S ACID-AMIDE ³⁴	42
FIGURE 3-1: <i>ENDO</i> -BICYCLO[2.2.2]OCTA-5-ENE-2,3-DICARBOXYLIC ANHYDRIDE 3	44
FIGURE 3-2: ACID-AMIDE SALT 6 WAS PREPARED, AND THIS WAS USED IN AN ATTEMPT TO SYNTHESISE THE AMIDE ESTER 8.	45
FIGURE 3-3: ACID-AMIDE 7	47
FIGURE 3-4: ACID-AMIDE 9	47

FIGURE 3-5: IMIDE 10	48
FIGURE 4-1: CONVERSION OF IMIDE TO ACID-AMIDE	57
FIGURE 4-2: GLÜSENKAMP'S ACID-AMIDE	58
FIGURE 4-3: KLUGER'S ACID-AMIDE.....	58
FIGURE A-1: GLYCOLYTIC PATHWAY	65
FIGURE B-1: PROTON NMR OF IMIDE 10.....	66
FIGURE C-1: GRAPH FOR DETERMINING ERROR OF K_{OBS}	67
FIGURE C-2: GRAPH FOR DETERMINING ERRORS OF K_R AND K_F	68
FIGURE D-1: GRAPH FOR DETERMINING ERRORS OF K_{LIM} AND pK_A	69
FIGURE E-1: EXAMPLE OF THE KINETIC ANALYSIS DATA.....	72
FIGURE E-2: TYPICAL REPETITIVE SCANNING SPECTRA FOR HYDROLYSIS OF ACID-AMIDE	73

List of Tables

TABLE 1-1: $T_{1/2}$ OF THE <i>N</i> -METHYLTRYPTAMIDES 1B-9B.....	14
TABLE 1-2: RATE CONSTANTS AND HALF LIVES OF ACID AMIDE AT DIFFERENT PH	18
TABLE 2-1: K_{OBS} VALUES OBTAINED AT VARIOUS $[OH^-]$	29
TABLE 2-2: K_{OBS} VALUES OBTAINED WITHIN THE PH RANGE OF 9-10.....	35
TABLE 2-3: K_{OBS} VALUES OBTAINED AT VARIOUS PH	38
TABLE 3-1: PREPARATION OF SOLUTIONS FOR KINETIC RUNS.....	50
TABLE 3-2: PREPARATION OF CARBONATE BUFFER SOLUTIONS (PH RANGE 9-10).....	52
TABLE 3-3: PREPARATION OF PHOSPHATE BUFFER SOLUTIONS (PH RANGE 5.5-7.5).....	53
TABLE 3-4: PREPARATION OF MALONATE BUFFER SOLUTIONS (SECOND IONISATION) (PH RANGE 4.5-8.5)	53
TABLE 3-5: PREPARATION OF MALONATE BUFFER SOLUTIONS (FIRST IONISATION) (PH RANGE 2-4).....	54

List of Abbreviations

ADEPT	Antibody-directed enzyme-prodrug therapy
ATP	Adenosine-5'-triphosphate
BuLi	Butyllithium
<i>d</i>	Doublet
<i>dd</i>	Doublet of doublets
DMAP	Dimethylaminopyridine
DMF	Dimethylformamide
DNA	Deoxyribonucleic acid
GDEPT	Gene-directed enzyme-prodrug therapy
HPLC	High performance liquid chromatography
IR	Infrared
K_a	Dissociation constant
KBr	Potassium bromide
k_f	Rate constant of forward reaction
k_{lim}	Limiting rate constant
k_{low}	Rate constant at higher pH plateau rate
k_{obs}	Observed rate constant
k_r	Rate constant of reversed reaction
<i>m</i>	Multiplet
Me	Methyl group
NMR	Nuclear Magnetic Resonance
pH _e	Extracellular pH
pH _i	Intracellular pH
ppm	Parts per million
<i>s</i>	Singlet
TAP	Tumour-activated prodrug
THF	Tetrahydrofuran
TLC	Thin-layer chromatography
$t_{1/2}$	Half-life
UV/Vis	Ultraviolet/visible
ϵ	Extinction coefficient
μ	Ionic strength

1 Introduction

1.1 Cancer

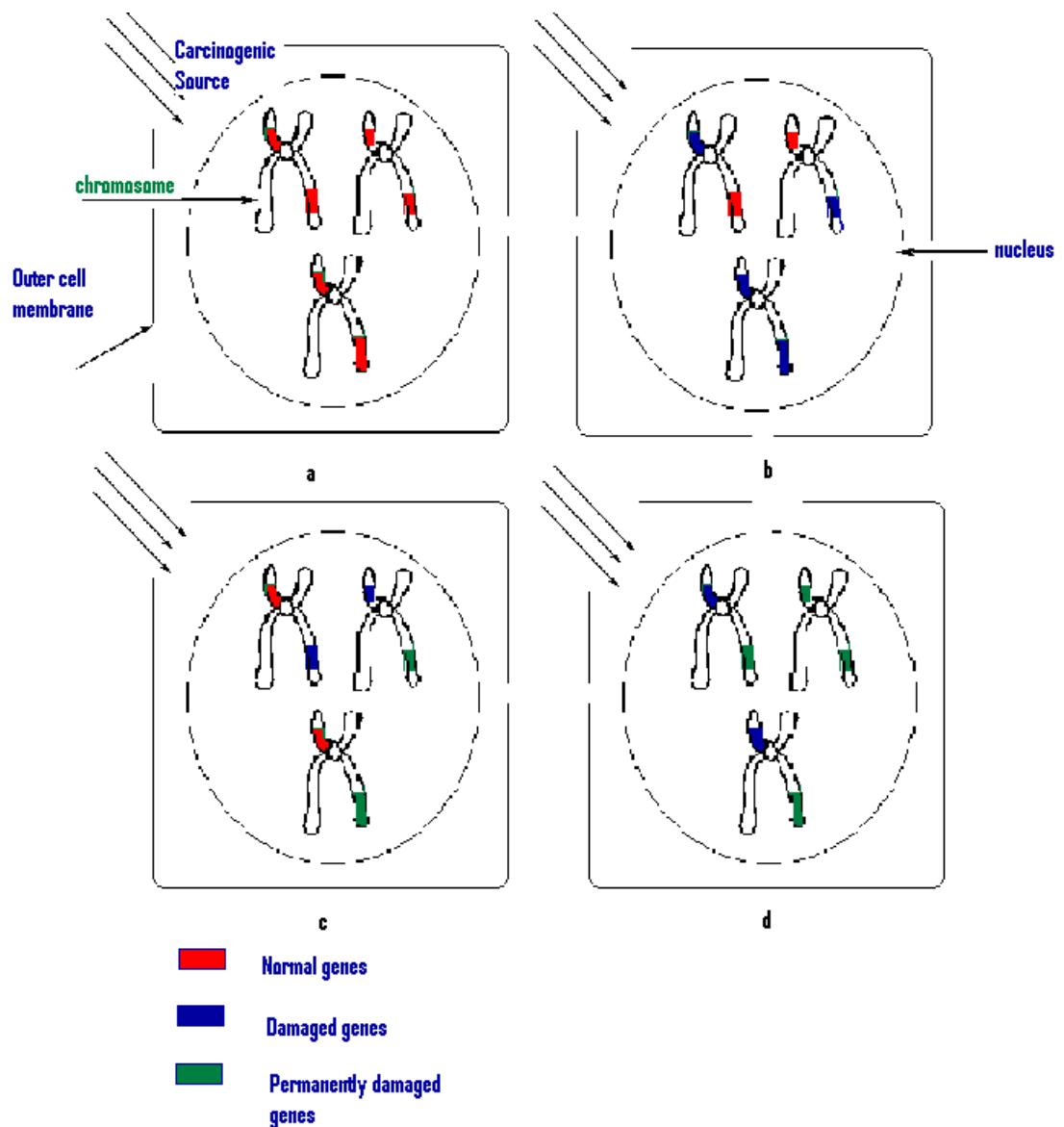
1.1.1 What is cancer?

A cancer is a growth or lump that damages surrounding tissues and organs, and that may spread to other parts of the body¹. It is not a single disease but a large group of disorders with different symptoms. Most cancers form tumour but some, like leukaemia, do not. However, nowadays, there is a grey zone between the terms cancer and tumour, which are being used interchangeably.

Today, cancer is a leading cause of death worldwide. This disease is accounted for 7.5 million deaths (around 13% of all deaths worldwide) in 2005 and it is predicted that 84 million people will die in the next 10 years if no further action is taken². Lung, stomach, colorectal, liver and breast cancer cause the most cancer deaths each year.

Cancer normally arises from one single cell transforming into a tumour cell. This is a result of the interaction between a person's genetic factors and other external agents, i.e. carcinogens. Carcinogens can bring damage to some specific genes known as oncogenes that regulate important cell process like cell division, growth, repair, and self-destruction of faulty cells. Some examples of carcinogens include smoke, industrial wastes, food by-products, and radiation.

Normally most damaged genes are repaired by the cell metabolism system, but eventually they can be altered or mutated if they are regularly exposed to carcinogenic sources. These damaged oncogenes can have altered versions of their chemicals within cells, and eventually the cell becomes cancerous (Figure 1-1).



- Normal cell being exposed to carcinogenic sources
- Some of the genes are eventually damaged with continuing bombardment of carcinogens.
- Newly-damaged oncogenes are usually soon repaired, but with time or continuous and/or high exposure to carcinogens, some of the oncogenes suffer permanent damages.
- With a few oncogenes being permanently altered, key cell functions are irreparably affected, resulting in a cancerous cell being formed.

Figure 1-1: Formation of cancerous cell by exposure to carcinogens

Ageing is another fundamental factor for the development of cancer². The incidence of cancer rises dramatically with age, most likely due to a build-up of risks for specific cancers that increases with age. The overall risk

accumulation is combined with the tendency of cellular repair mechanisms to be less effective as a person grows older.

All cancers begin with a single normal cell, converting from a normal state to an abnormal cancerous state. During this process, the cells acquire three main malignant properties that distinguish them as cancer cells³:

1. An uncontrolled growth/division beyond their usual boundaries
2. A diminished ability to undergo apoptosis
3. An ability to spread (from the site of origin)

An uncontrolled growth/division

As in every normal cell, cancer cells have the ability to divide among themselves to form large clusters of cells. When a normal cell is transformed into a cancer cell, it multiplies until tumours are formed and can be ultimately detected. It is generally thought that one billion cancer cells need to have formed before a cancer can be detected.

The difference between a normal growth and a cancer growth is that normal growth happens in a controllable and precisely timed manner, whereas cancer cells divide freely without any restraints. This property has been taken into account by many medical researchers in the development of cancer treatment methods. Since the cancer cells are more actively dividing than the normal cells, they are therefore more readily being exposed to certain chemotherapies and radiation treatments.

It has to be aware that although cancer cells are growing in an uncontrollable manner, this does not necessarily mean that cancer is always caused by cells “growing out of control” or “running amuck”. There are some types of cancers, especially true in the case of solid tumours, do not grow like wildfire but at a very slow rate – in some cases slower than the normal cell divisions. The dominant problem with this kind of tumour is mostly due to the cells’ “near-immortality”, which leads to the second malignant property of the cancer cells.

A diminished ability to undergo apoptosis

Every cell has a finite, predetermined life span, either long or short. To maintain the balance of numbers of cells in the body, a system – encoded in every single cell's DNA (deoxyribonucleic acid) - exists to eliminate the diseased, defective and old cells, replacing them with the new ones. This system operates through a process called apoptosis, which causes the cells' internal parts to dissolve leading to cell suicide. In Greek, *apoptosis* means falling off, as in leaves from a tree or petals from a flower.

The concept of apoptosis is very important here because it is well known that cancer cells have a diminished ability to undergo apoptosis in which they are supposed to be eliminated naturally. This occurs because they have an altered genetic programme of apoptosis brought by DNA mutations, i.e. change in nucleotide sequences of the genetic material. This results in the switching-off of apoptosis process in cancer cells, leading to infinite growth of tumour mass.

An ability to spread from the site of origin

Another important concept in oncology is metastasis. This is the process in which the cancer cells spread from the site of origin, called the “primary” site, to other locations in the body, called “metastatic” or “secondary” sites.

At the primary site the cells get loosen and eventually dissolve the forces that bind them to their neighbouring cells. The freed cells can then enter the bloodstream or lymphatic channels and travel to the metastatic sites by forming new blood vessels – a process named “angiogenesis” – to gain access to the blood circulation.

Normally each type of cancer has its associated “preferred” metastatic sites. By gaining knowledge of these sites the initial assessment of the extent of disease can thence be carried out.

1.1.2 Types of Cancer

There are hundreds of distinct types of cancer, while each is grouped into four main categories³:

1. Carcinomas – Cancers derived from epithelial cells.
2. Hematologic malignancies – These cancers are related to the blood and lymph systems in the body (*hema* is Greek for blood). They cause alterations of blood counts, enlargement of lymph nodes, or defects in the body's immune defences, resulting in infections. The most commonly known cancer from this type is leukaemia which does not form tumours.
3. Sarcomas – Derived from the supporting structures, including muscle, bone, cartilage, fibrous tissue, fat, nerves, and blood and lymphatic vessels, of the body (*sarc-oma* is Greek for “fleshy growth”).
4. Brain tumours – These occur in the central nervous system, protected by a barrier of bones and membranes and bathed in spinal fluid. Unlike the other types of cancers, they do not spread to the rest of the body.

1.1.3 Treatments targeting cancer cells

Some of the conventional cancer therapies include^{3, 4}:

- Surgery
- Radiotherapy – Using radiation to kill cancer cells and to shrink tumours by damaging the genetic material in the cells and stops them from multiplying.
- Chemotherapy – Using drugs to interfere with the ability of cancer cells to proliferate.
- Targeted therapy – Targeting the receptors, signalling molecules and/or angiogenesis process to disrupt cancer cell growth.
- Hormonal therapy – Using drugs to block the production of hormones responsible for growth of cancer, e.g. oestrogen or testosterone the reproductive organs.

- Cryotherapy – Using extreme cold – e.g. nitrogen probes - to destroy cancer cells.
- Brachytherapy – By implanting catheters, needles, capsules or seeds containing radioactive materials to kill cancer cells.

1.2 Tumour-Activated Prodrug

1.2.1 Disadvantages of most anticancer drugs today

As mentioned above, chemotherapy uses drugs to stop cancer cells from proliferating. It is well known today that a lot of these drugs can bring some side effects to at least some level to the cancer patients. These side effects include hair loss, vomiting and nausea, to name a few.

The majority of the clinically-used anticancer drugs today are systemic cytotoxins that kill the cancer cells primarily by attacking their DNA. On one hand these drugs are efficient to kill large number of cancer cells with constant proportion kinetics – many exhibit a log-linear relationship between carcinoma cells and drug concentration⁵; on the other hand they are not truly selective to the cancer cells that their therapeutic efficacy is highly limited by the damage they cause to the normal cells which might be essential for life. This can be a major concern especially in the case of treating solid tumours which are dividing relatively slow compared to the normal cells.

As a result, not only the anticancer drugs have very limited benefits to treat the cancer, they are also bringing more of other damages to the body of the patients. To solve this problem and increase the clinical efficacy of the anticancer drugs, one way is the use of relatively non-toxic prodrug forms that can be selectively activated in tumour tissue.

1.2.2 Prodrugs

Prodrugs can be defined as agents that are transformed after administration, either by metabolism or spontaneous chemical breakdown, to form pharmacologically active species⁶. About 5-7% of drugs approved worldwide today can be classified as prodrugs⁷.

The efficacy of anticancer drug is generally directly dependent on the drug concentration as well as its time of exposure. Deactivating the drug as a prodrug until needed at the site of action is extremely useful – and quite commonly used - to improve the solubility, transport and pharmacokinetic properties of the anticancer agents⁸.

1.2.3 Tumour-activated prodrugs

There is an increasing interest in developing tumour-activated prodrugs (TAPs) which are aimed at increasing the selectivity of the prodrugs to kill the cancer cells, leaving the rest of the normal cells unharmed.

A TAP design must fulfil certain requirements. First, they must be able to be delivered to the distant regions in tumours, and thereby be selectively activated to generate a cytotoxic species to kill the tumour tissues only. Second, they must be capable to produce a “bystander effect” - the ability to diffuse a limited distance to kill neighbouring tumour cells that may lack the ability to activate the prodrug⁶. This is a crucial requirement because in many cases only a small proportion of tumour cells is likely to possess the ability to activate a prodrug.

A modular approach to the design of TAP is to have a molecule consists of three domains: trigger, effector and linker units (Figure 1-2)⁶. The linker, acting as an inter-bridge linking the trigger and effector units, deactivates the prodrug until the trigger unit undergoes a metabolism carried out by one of the tumour-specific mechanisms. The linker then rapidly transmits

the change to the effector, which destroys tumour cells rapidly and under all conditions of pH and cell cycle status.



Figure 1-2: General layout of a tumour-activated prodrug (TAP) design

A TAP can be selectively activated via various mechanisms, mainly based on:

- i. Tumour physiology - e.g. selective enzyme expression, hypoxia and pH differences.
- ii. Drug delivery techniques - e.g. antibody-directed enzyme-prodrug therapy (ADEPT) and gene-directed enzyme-prodrug therapy (GDEPT).

In this context we will be focusing on the activation of TAP by the pH-differences between tumour and normal tissues.

1.2.4 pH-sensitive TAPs

There have been very few well-documented consistent differences between normal cells and tumour cells, one of them being the pH differences – tumour tissues are found to have lower extracellular pH (pH_e) values than the normal tissues⁹.

The expanding population of tumour cells often lead to insufficient nutritional supplies by the functional vasculature system, leading to deficiency of oxygen. Hence under anaerobic conditions lactic acid is produced, together with the hydrolysis of adenosine-5'-triphosphate (ATP) in an energy-deficient environment, giving a relatively more acidic environment in tumour tissues. It is therefore commonly believed that hypoxia and acidity co-exist in the microenvironment of tumour tissues.

Warburg¹⁰ found that tumour tissues depended greatly on glycolysis for a source of metabolic energy, and hence proposed in 1923 that these cells had impairment of respiration system. As a rule, one mole of breathed oxygen causes the disappearance of 1-2 mole of lactic acid. Warburg's hypothesis was based on the fact that the respiration does not cause the glycolysis to disappear in tumour tissues.

This hypothesis was later proved to be wrong, as tumour tissues were showed to be fully able to use respiration as a source of metabolic energy. Weinhouse¹¹ claimed that the reason for the persistence of glycolysis in oxygen is that it is so high in tumours that a normal respiration and a normal Pasteur effect are incapable of eliminating it. It is thus believed that the tumour cells use anaerobic glycolysis as primary source for obtaining metabolic energy due to the existence of hypoxic regions in which oxygen is not available for respiration process.

Glycolysis is also referred as the Embden-Meyerhof pathway (refer to Appendix A for the complete pathway). Under anaerobic conditions, 2 mol of lactic acid and 2 mol of ATP are produced for every mol of glucose consumed. The production of protons via the ATP hydrolysis here is thought to be the major cause of acidity in tumours, although additional pathways may also lead to acid production.

A poor chaotic tumour vascularisation often leads to an inefficient removal of the acidic products and contributes further to development of the chronically acid extracellular environment¹².

In a cell, there is a constant loading of acid, which is generated metabolically and through passive diffusion of H^+ (equivalents), due to the internally negative membrane potential. As pH_i has to be maintained above the equilibrium pH^{13} , it is closely regulated by recruiting some H^+ -consuming mechanisms to transport these proton ions to the extracellular

space of the cell during aerobic/anaerobic glycolysis, glutaminolysis, and ATP hydrolysis processes.

Some major transport mechanisms responsible for regulation of pH_i in acid-loaded cells include the Na^+/H^+ antiport and the Na^+ -dependent $\text{HCO}_3^-/\text{Cl}^-$ exchanger. Other membrane transporters, such as H^+ -ATPase pumps, lactate:proton symport, and increased turnover of acidic vesicles, may also contribute to the regulation of pH_i by extruding protons from cells^{9, 12-14}. Via the interstitial space these proton ions are removed from the tissues through the blood vessels by convective transport.

Rapidly growing tumours usually have a high metabolic rate and a high lactic acid production (as discussed previously). If these conditions coincide with an insufficient proton removal system, the proton ions accumulate in the tissues and give a lower pH_e values. Thus the active regulation of pH_i has highlighted the problem of tumour pH_e/pH_i differential.

Investigations carried out by Newell *et al.*¹⁵ indicate that solid tumours derived from glycolysis-deficient cells do not accumulate lactic acid above serum levels yet are as acidic as parental tumours. They proposed that the acid production is due to the poor removal of CO_2 produced by inadequate tumour vasculature, allowing sufficient time for the hydration of CO_2 to carbonic acid H_2CO_3 and hence giving a net H^+ production within solid tumours. Further experiments are however necessary to evaluate this finding.

pH_e is conventionally measured by insertion of pH electrodes, whereas intracellular pH (pH_i) is more conveniently measured by ^{31}P -NMR spectroscopy techniques. Wike-Hooley *et al.*¹⁶ had done a comprehensive review of several thousand microelectrode measurements of pH in human and animal tumours, which summarised that tumours are more acidic than normal tissues with median pH values of about 7.0 in tumours and 7.5 in normal tissues. Investigations carried out by Vaupel *et al.*¹⁷ also showed that for C3H mouse mammary carcinomas, most of the measured pH

values are in the range of 6.4 to 7.1, with an absolute value as low as 5.8 observed in large ulcerated tumours.

Thus, cell-excluded prodrugs those are able to be selectively activated at the lower-than-normal pH_e occurring in tumour tissues, releasing potent cytotoxins that can enter cells, have significant theoretical advantages as anticancer drugs.

However, relatively little work has been reported on prodrugs of this type, mainly because the pH difference involved is not large, at maximum perhaps 1 unit (from the pH 7.4 in normal tissues down to about pH 6.5 in severely hypoxic regions of solid tumours⁹). It is therefore necessary to find chemistries that are sensitive to small pH changes.

One approach is to construct prodrugs containing amine cytotoxins present as amide functions but designed to be released when the amide undergoes hydrolysis, and hopefully getting a rate differential significantly in favour of pH 6 over pH 7. Amides generally are non-reactive in hydrolysis at physiological pH but neighbouring un-ionised carboxylic acid groups provide dramatic catalysis by cyclisation to release amine (see section 1.3).

Normal acids have pK_a values of around 4-5 so the challenge is to find compounds containing acid groups which are still incompletely ionised at around pH 6. A system with a higher absolute reaction rate because of structural or conformational constraints on orientation of the acid and amide groups is also required.

1.3 Amide Hydrolysis

Under physiological conditions the hydrolysis of amides exhibits half-lives of about 7 years, as investigated by Kahne *et al.* using a radioassay experiment at neutral pH and room temperature¹⁸. There are however a few papers that reported on enhanced hydrolysis rates for some amides, such as Bender's phthalic acid amide ($t_{1/2}$ of 49 minutes and 17.5 hours at pH 3.0 and 5.0, respectively, at 47.5°C; 10^5 faster than the corresponding benzamide)¹⁹, *N*-*n*-propyldiisopropylmaleamic acid ($t_{1/2}$ less than 1 second at 39°C below pH 3)²⁰, and Menger's peptidase model (Figure 1-3) ($t_{1/2}$ 8 minutes at 21.5°C at pD 7.05)²¹.

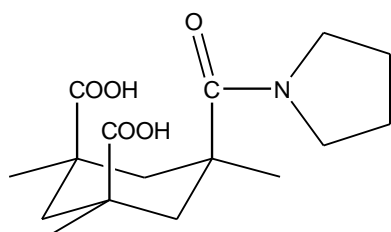


Figure 1-3: Menger's peptidase model

The amide hydrolysis is initiated by proton transfer from the adjacent carboxyl group to the amide, followed by intramolecular nucleophilic attack of the carboxylate ion to the carbonyl carbon atom of amide²². This is illustrated following (Figure 1-4) using an example of the hydrolysis of *N*-methylphthalamic acid which gives the corresponding anhydride and amine molecule²³. The anhydride subsequently hydrolyses with water.

The hydrolysis reaction is at a maximum rate when the acid group is in an un-ionised -COOH form (c.f. in the ionised -COO⁻ form), and slows with degree of ionisation as the pH increases.

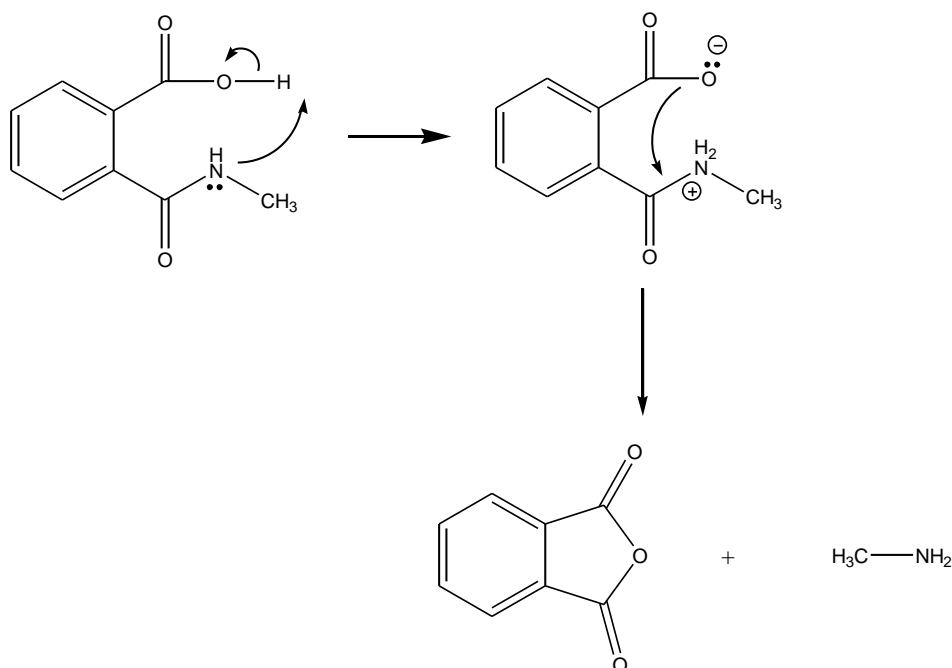
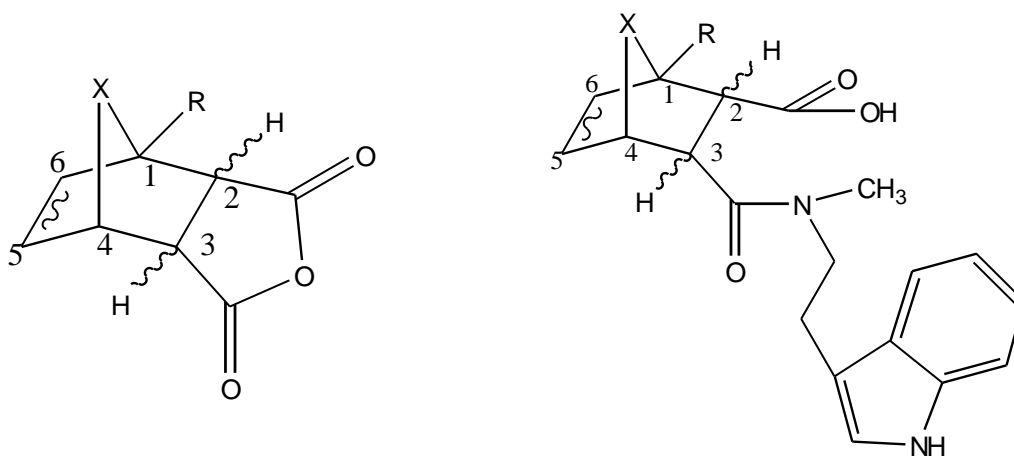


Figure 1-4: Hydrolysis of *N*-methylphthalamic acid

1.3.1 Glüsenkamp's Investigations

Glüsenkamp and co-workers had synthesised a class of bicyclic carboxyamides **1-9b** (Figure 1-5) differing with respect to substitution patterns and exo-endo geometry²². They used *N*-methyltryptamine and bicyclic anhydrides as precursors for these acid labile amides. The highly substituted bicyclic anhydrides were used as they offer great structural varieties with potential for rate enhancements, and might be used as tools for masking and modifying therapeutic agents containing the amine functionalities.

The cleavage rate of the amide bonds was shown to be proportional to the degree of protonation of the neighbouring carboxyl group, which is related to the correspondent structure-related dissociation constants (K_a)¹⁹⁻²¹. Thus the correlation between cleavage rates and substitution patterns were studied by performing the kinetic experiments under identical reaction conditions but at different pH values (Table 1-1).



- 1a, 1b;** X=O; R=CH₂-O-COPh; 2, 3-*exo*; 5, 6-CH
2a, 2b; X=O; R=CH₂-O-COPh; 2, 3-*exo*; 5, 6-CH₂
3a, 3b; X=O; R=CH₂-O-COPh; 2, 3-*endo*; 5, 6-CH
4a, 4b; X=O; R=CH₂-O-COPh; 2, 3-*endo*; 5, 6-CH₂
5a, 5b; X=O; R=H; 2, 3-*exo*; 5, 6-CH
6a, 6b; X=O; R=H; 2, 3-*exo*; 5, 6-CH₂
7a, 7b; X=CH₂; R=H; 2, 3-*endo*; 5, 6-CH
8a, 8b; X=CH₂; R=H; 2, 3-*endo*; 5, 6-CH₂
9a, 9b; X=CH₂-CH₂; R=H; 5, 6-CH₂

Figure 1-5: Glusenkamp's bicyclic anhydrides (a, left) and their corresponding *N*-methyltryptamine derivatives (b, right) as model amides

Table 1-1: $t_{1/2}$ of the *N*-methyltryptamides 1b-9b

Compound	pK _a	$t_{1/2}$ [min] (pH 5.0)	$t_{1/2}$ [min] (pH 6.0)	$t_{1/2}$ [min] (pH 7.0)
1b	4.6	67	336	2340
2b	4.6	17	106	840
3b	4.7	312	1560	12480
4b	4.5	155	930	7440
5b	4.5	31	159	1260
6b	4.6	10	52	420
7b	5.4	2	13	102
8b	5.4	2	13	102
9b	5.9	0.3	0.5	2.4

In the study the cleavage rates (k_{obs}) were determined by high performance liquid chromatography (HPLC) and ultraviolet spectroscopy at 37°C and 150 mM salt concentration at different pH values; the half-lives ($t_{1/2} = 0.693/k_{\text{obs}}$) were calculated according to *pseudo*-first order kinetics.

The data revealed that all oxygen-bridged ring systems exhibit comparable pK_a values of 4.5-4.7. On the other hand, the amides **7b** and **8b** show pK_a values of 5.4, and the amide **9b** (Figure 1-6) exhibits an unusual high value of 5.9. The comparison of half lives ($t_{1/2}$) clearly shows a strong structure-dependent lability. Glüsenkamp thus summarised that, in general:

1. *Exo*-compounds are more reactive than their corresponding *endo*-compounds.
2. Saturated, oxygen-bridged structures are generally about 2-3 times more labile than the corresponding unsaturated compounds (compound **6b** vs. **5b**).
3. Substitution of the oxygen by an ethane bridge (-CH₂-CH₂-) results in a dramatically increased cleavage rate. The carboxyamide **9b** exhibits an extremely short half-life of only 0.3 minutes at pH 5.0, and 2.4 minutes at pH 7.0.

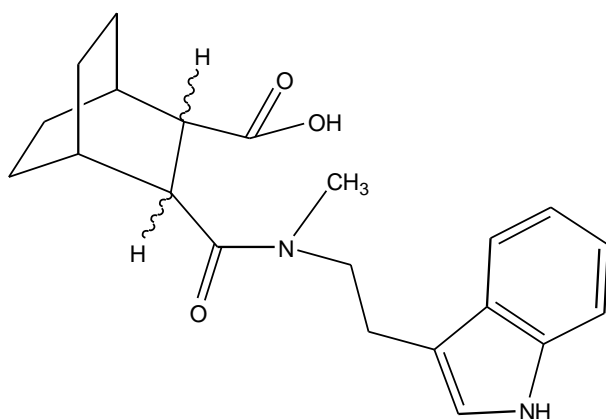


Figure 1-6: Glüsenkamp's acid amide **9b** - high hydrolysis rate

1.4 Previous work

Prior to the current master's project, a preliminary short undergraduate project²⁴ was carried out in our laboratories using a secondary amine. The acid-amide prepared was not obtained in a pure form due to time constraints, but it was used as an impure salt for a preliminary assessment of pH-rate profile for the hydrolysis reaction.

The preliminary work was carried out with the following aims:

1. To synthesise a ring-unsaturated analogue of Glüsenkamp's most reactive acid amide **9b**
2. To determine the hydrolysis rate of the synthesised compound and its pH-sensitivity in hydrolysis reaction.

For the acid-amide synthesis (Figure 1-7), *N*-methylaniline was chosen as the secondary amine, whereas the bicyclic anhydride was prepared from maleic anhydride and 1,3-cyclohexadiene via a Diels-alder reaction. Reaction of the *endo*-bicyclic anhydride with the lithium amide gave an impure lithium salt of the acid-amide (analysis by nuclear magnetic resonance spectroscopy).

Although a pure product could not be obtained within the shortest time-frame of the study, the impure salt was used for preliminary assessment of pH rate profile of its cyclisation to release *N*-methylaniline (Figure 1-8). This was established by measuring its rate of reaction at different pH values (in the range of pH 5.7 to 7.2). This was done by ultraviolet/visible (UV/Vis) scanning after addition of aliquots of an aqueous solution of the acid-amide salt **6** to the buffered phosphate aqueous solutions at 30°C.

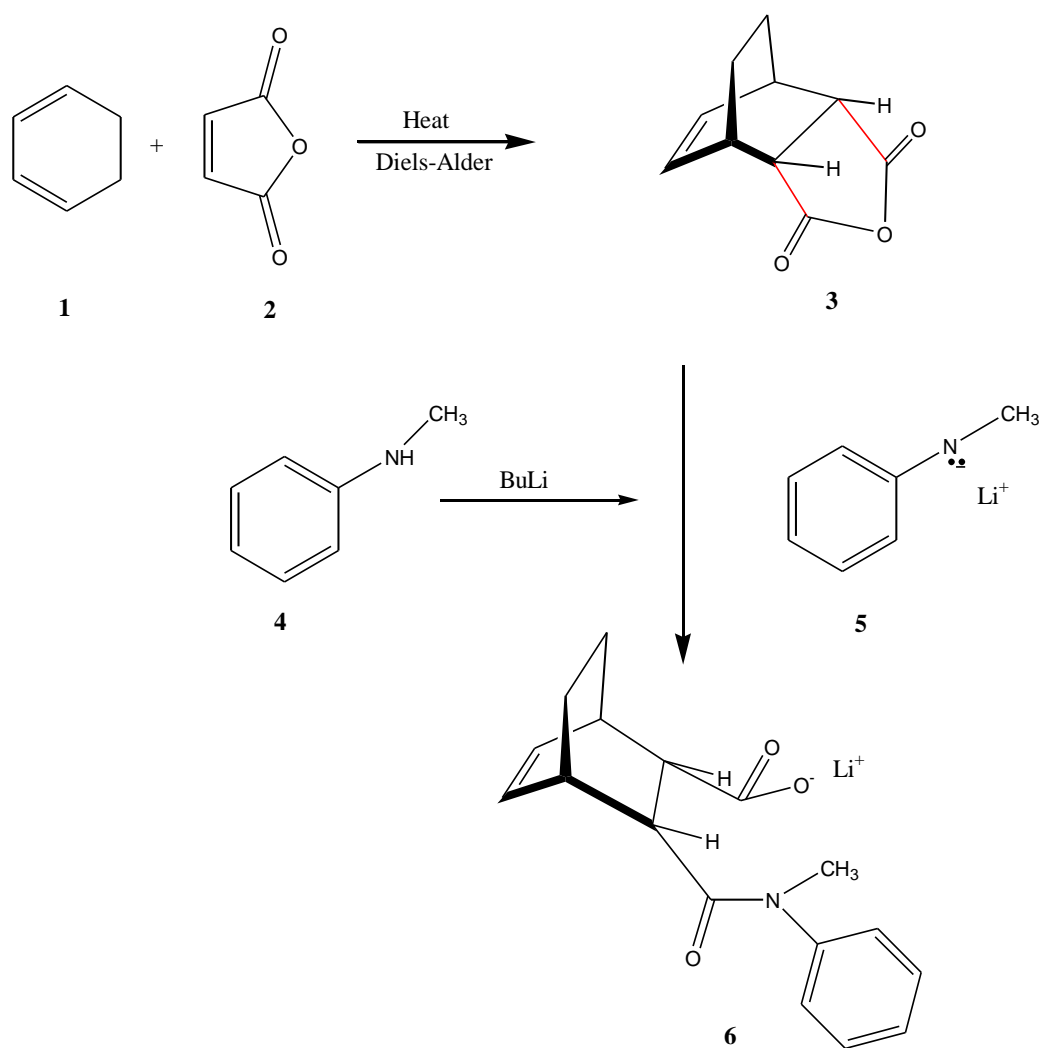


Figure 1-7: Synthetic route to acid-amide

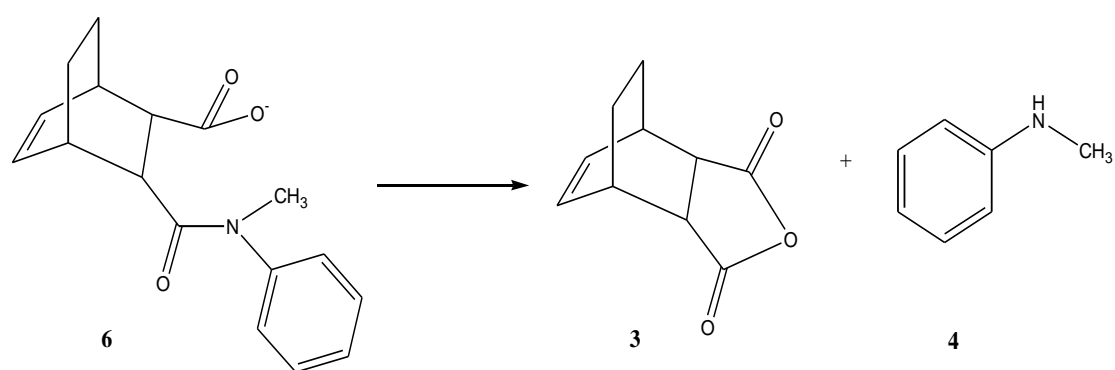


Figure 1-8: Cyclisation of acid-amide to release amine

The increasing absorbance at 238 nm and 288 nm was consistent with the formation of *N*-methylaniline, and the absorbance values at 238 nm were read off at certain time intervals. From these, a graph of $\log_{10}(A_{\infty}-A_t)$

against t was plotted, and the first order rate constants and half-lives calculated. The results, summarised in the following table and graph, are however subject to uncertainty because of the known lack of purity of reactant.

Table 1-2: Rate constants and half lives of acid amide at different pH

pH	Rate Constant k (min^{-1})	$t_{1/2}$ (min)
7.2	0.012	56
6.4	0.039	18
6.0	0.083	8
5.8	0.108	6
5.7	0.119	6

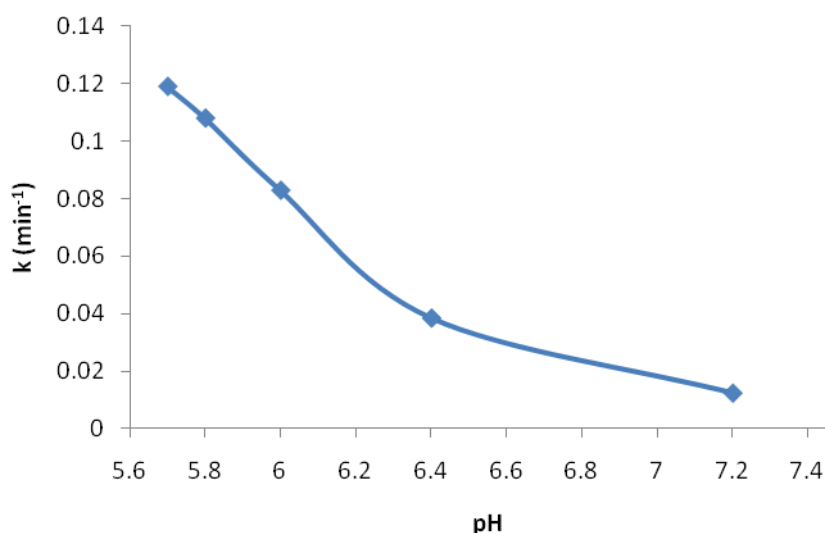


Figure 1-9: pH-rate profile of acid-amide

From the graph, with decreasing pH the reaction rate increases, indicating that the amide cyclisation reaction is faster at lower pH compared to high pH values.

The reaction half life was about 56 minutes at pH 7.2, and 6 minutes at pH 5.7. The results seemed to have attained the initial aim of releasing *N*-methylaniline at a rate differential significantly in favour of pH 6 over pH 7;

but more thorough investigations with pure acid-amide would be needed to obtain more reliable results.

1.5 Project Aim

For the directed study research, the acid-amide was only synthesised in its salt form, and the product was not purified to give accurate rate measurements with pH. This synthesis difficulty seemed to be associated with the use of sterically crowded secondary amine (*N*-methylaniline), so for the current study it was replaced with a primary aromatic amine, *p*-methoxyaniline.

Thus, the goal of the current master's project was to synthesise the acid-amide in its un-ionised form, purify it, and to obtain a full pH-rate profile for its cyclisation. In the event purity problems required it to be synthesised by an indirect route through the corresponding imide.

2 Results and Discussions

2.1 Preparation of *endo*-bicyclo[2.2.2]octa-5-ene-2,3-dicarboxylic anhydride 3

This synthesis is by the well-known Diels-Alder cycloaddition pathway reported in many research papers²⁵⁻²⁸. In this project, the method of preparing the *endo*-anhydride was adapted from Birney *et al.*²⁸

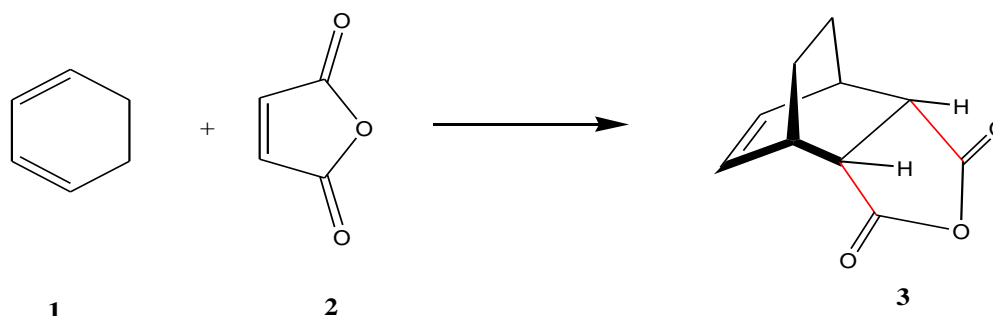


Figure 2-1: Synthesis of *endo*-bicyclo[2.2.2]octa-5-ene-2,3-dicarboxylic anhydride

The words *endo* and *exo* are used to indicate relative stereochemistry when referring to bicyclic structures. A substituent on one bridge is said to be *exo* if it is *anti* (*trans*) to the larger of the other two bridges and is said to be *endo* if it is *syn* (*cis*) to the larger of the other two bridges²⁹ (Figure 2-2).

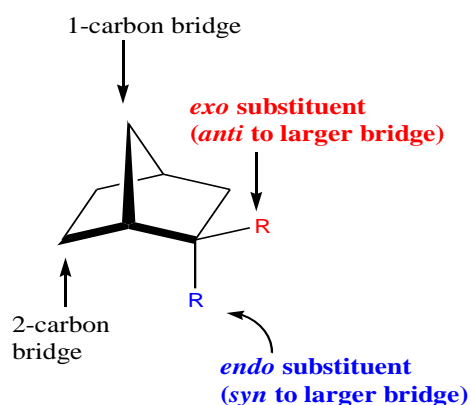


Figure 2-2: Definition of *endo* and *exo* substituent

The diene (1,3-cyclohexadiene) and dienophile (maleic anhydride) preferentially line up to form the *endo* product, rather than the alternative *exo* product, because of the more favourable orbital overlap between

diene and dienophile when the reactants lie directly on top of one another with the electron-withdrawing substituent on the dienophile underneath the diene²⁹ (Figure 2-3). This stereoselectivity is one of the unique features of the Diels-Alder reaction, but is lost at higher temperatures when there is a chance of reversibility occurring, and the more stable *exo* product may be formed.

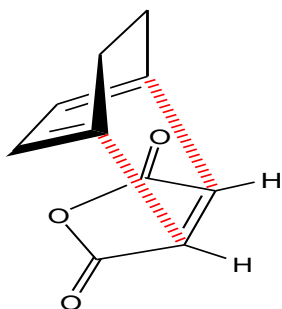


Figure 2-3: Formation of the *endo*-product via Diels-Alder cycloaddition reaction

Birney *et al.* recrystallised the crude *endo*-anhydride from methanol and obtained a product yield of 82%. However, when the Birney method was attempted, less than 30% of the expected yield was obtained, and the infrared (IR) spectrum suggested the presence of an acid-ester group. One possible reason for this could be that methanol reacted with one of the C=O carbonyl groups of anhydride to give an acid-ester, thence lowering the yield of pure anhydride that recrystallised out from methanol.

The crude *endo*-anhydride was later recrystallised from dichloromethane instead of methanol. Even though the yield was not as high as the 82%-yield reported by Birney, the acid-ester peak was no longer observed on IR spectrum, and the IR analysis and melting point determination confirmed that the desired *endo*-bicyclic anhydride had been successfully prepared.

In the following sections, the *endo* stereochemistry of reactants and products is for simplicity not indicated but should be assumed.

2.2 Attempted syntheses of acid-amide using *N*-methylaniline

2.2.1 Introduction

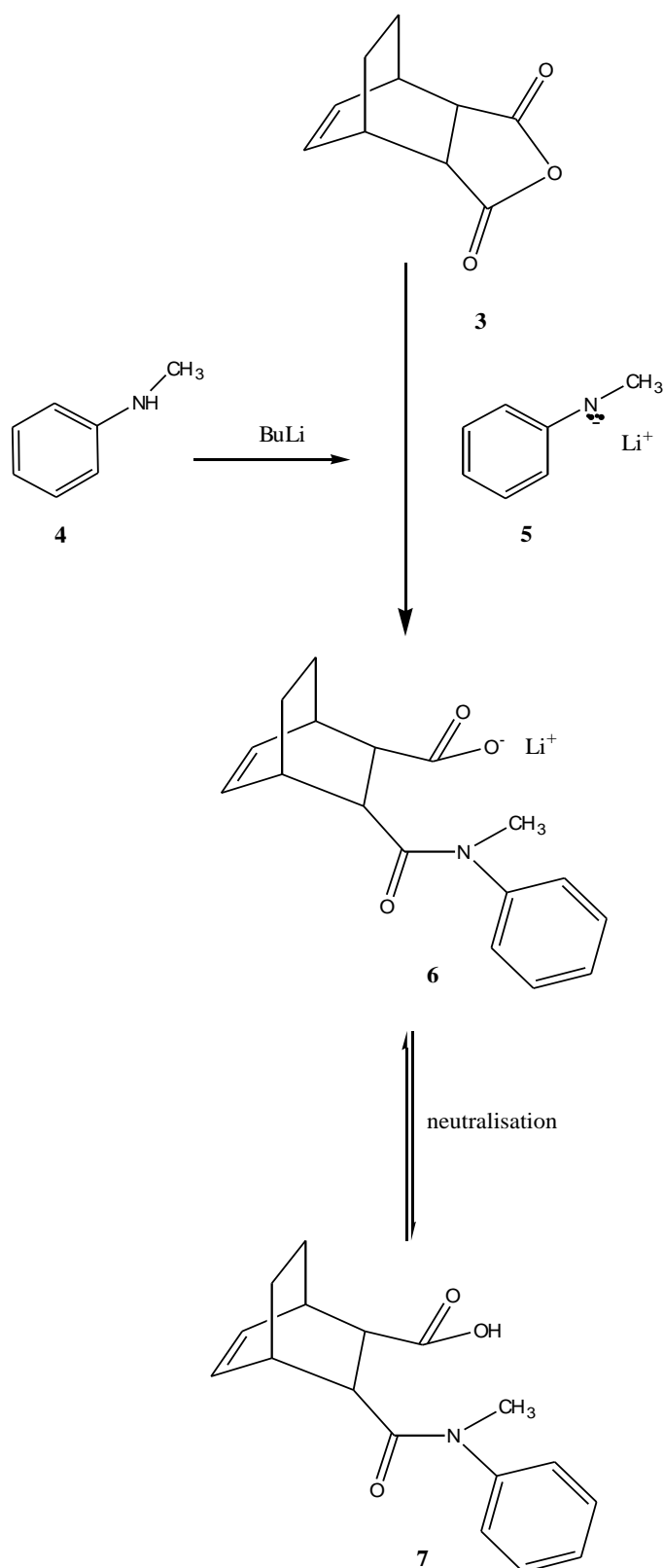


Figure 2-4: Synthesis route to acid-amide 7

Figure 2-4 shows an initial attempt to prepare a secondary acid-amide **7** using *N*-methylaniline. The amide salt **6** was prepared by first ionising *N*-methylaniline **4** with butyllithium, after which the product **5** was reacted with *endo*-anhydride **3** to give **6**.

Previous work done by Menger *et al.* on Kemp's acid amides suggests that acid-amide **7** may be too reactive to isolate in the neutral form²¹. Meanwhile, an earlier study²⁴ had also indicated that a pure product of **6** was difficult to prepare. Therefore, the neutralisation step (**6** → **7**) was not carried out. Instead, an attempt was made to "trap" **6** as an ester which could be purified and then hydrolysed to get a pure sample of a secondary acid-amide (Figure 2-5).

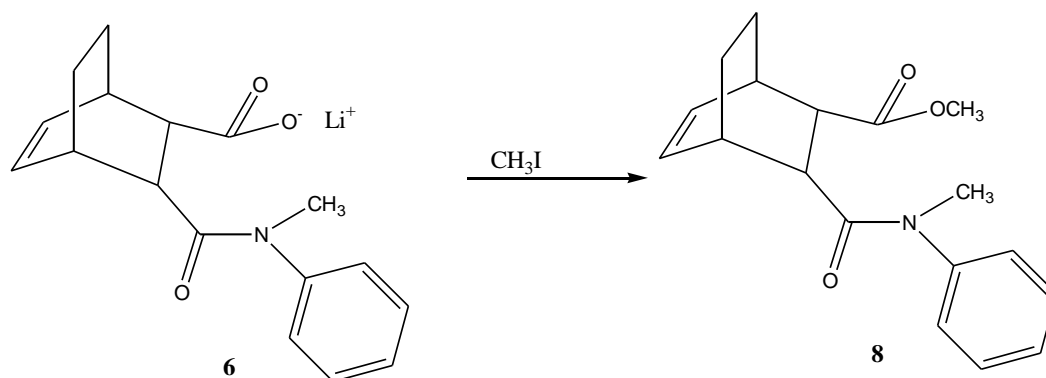


Figure 2-5: Esterification of acid-amide salt 6

The main reason for using *N*-methylaniline was that most cytotoxins used in anticancer treatments today are arylamines but not aliphatic amines^{21, 30}. Moreover, *N*-methylaniline is a secondary amine so the product cannot form an imide in an unwanted side-reaction. If a primary amine like aniline is used, the acid-amide would be formed but might also form some imide in competition with hydrolysis³¹ (Figure 2-6). This would subvert the reason for forming the acid-amide in the first place, i.e. to release the amine by hydrolysis reaction.

When the amide ester **8** was not successfully prepared, another attempt was made to prepare acid-amide **7** directly from *endo*-anhydride **3** in 1,4-dioxane, a high boiling point solvent (Figure 2-7).

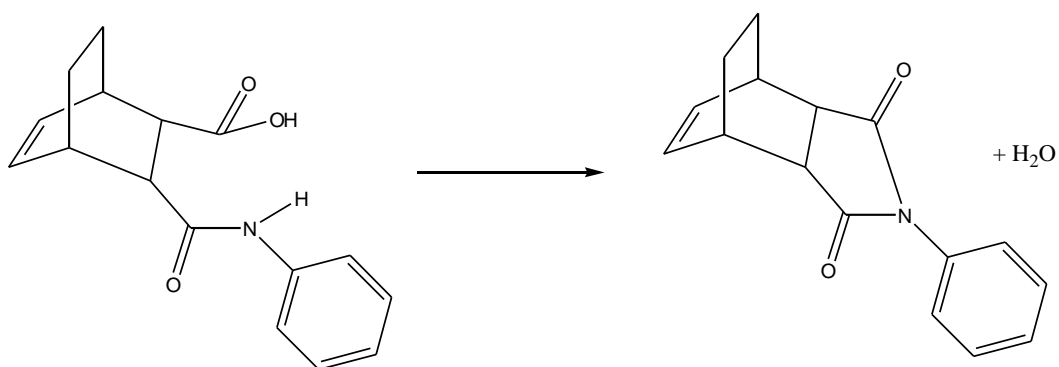


Figure 2-6: Formation of imide due to use of a primary amine

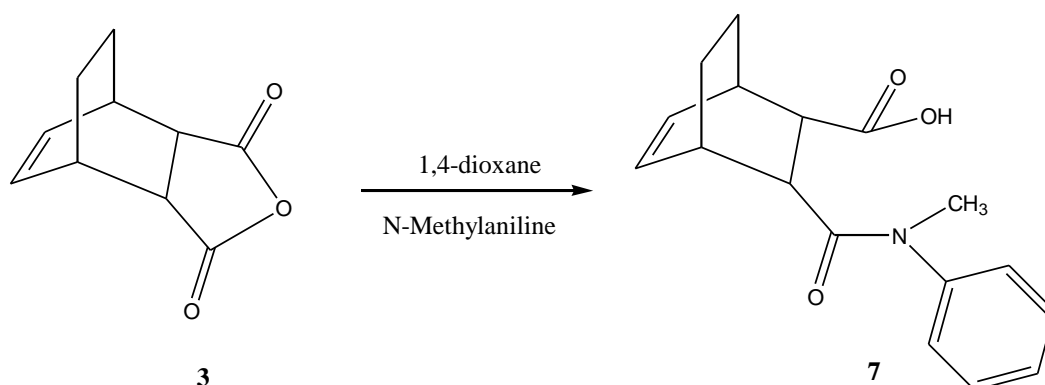


Figure 2-7: A direct synthesis of acid-amide 7 from *endo*-anhydride 3

2.2.2 Attempted synthesis of amide ester 8

Acid amide **6** was reacted with methyl iodide and K_2CO_3 in acetone (dried with 4 Å molecular sieves prior to use). K_2CO_3 does not dissolve in acetone but forms potassium iodide, KI, over time as iodide substitution occurs. K_2CO_3 acts as a base and is expected to exchange Li^+ for K^+ , thus making the carboxylate ion COO^- more reactive. However, after the reaction was left for more than 24 hours, there were no signs of products being formed by thin-layer chromatography (TLC). NMR and IR analysis could not confirm the formation of **8**. The same applied in a second attempt in which the acetone was replaced by dimethylformamide (DMF) as the reaction solvent.

2.2.3 Direct synthesis of acid-amide 7

1,4-dioxane is classified as an ether, but more polar in structure and with a high boiling point. Prior to use, it was treated with activated alumina which acts as a water-adsorbent to ensure the solvent was water-free and removes any peroxide impurities.

After the reaction was reflux for 16 hours, no product seemed to be formed as shown by TLC analysis. Dimethylaminopyridine (DMAP) was later added to act as a base catalyst to aid the esterification process. Even so, no reaction was observed. Steric factors are assumed to thwart the reaction of the secondary amine.

2.3 Attempted synthesis of acid-amide using *p*-methoxyaniline

2.3.1 Introduction

As the attempt of preparing an acid-amide using *N*-methylaniline had not been successful, the synthetic plan was changed to replace *N*-methylaniline with *p*-methoxyaniline, a less sterically hindered primary amine molecule. However, the synthesis of the primary acid-amide was not successful as a pure compound could not be obtained. The plan had thus again to be diverted in this case to synthesising an imide, purifying it and then opening the imide ring in KOH to get a pure acid-amide carboxylate salt solution which could be used for kinetic analyses by adding aliquots to lower pH buffer solutions.

2.3.2 Synthesis of acid-amide 9

p-Methoxyaniline was reacted with *endo*-anhydride to give crude acid-amide **9**. The *endo*-anhydride was difficult to dissolve in ether at room temperature; hence it was dissolved with heating. IR analysis of the product gave carbonyl peaks at 1731 and 1649 cm⁻¹ which are consistent with the presence of a carboxylic acid and an amide group, respectively.

Absorbance at 1780 cm^{-1} however indicated presence of some residual anhydride.

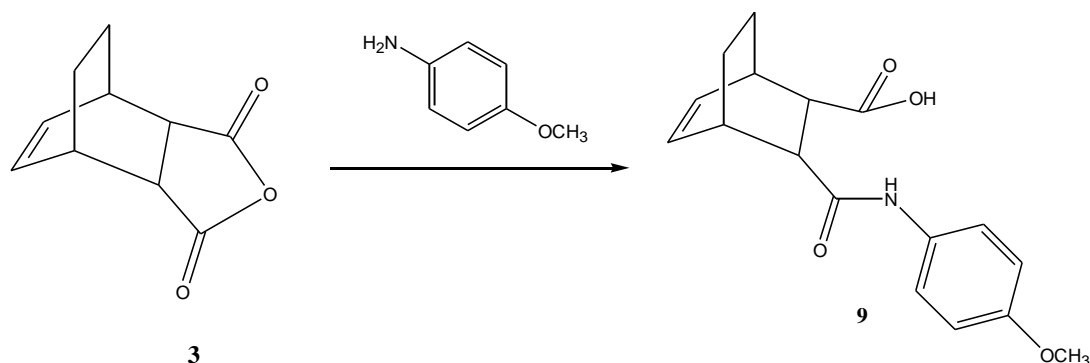


Figure 2-8: Synthesis of acid-amide 9

The reaction of crude **9** was studied in 0.1 mol L^{-1} phosphate buffer solution ($4:1\text{ H}_2\text{PO}_4^-/\text{HPO}_4^{2-}$) at pH 6.4 by repetitive UV (ultraviolet) scanning to completion. The UV spectrum showed a decreased absorbance at 250 nm, indicating that acid-amide **9** was being hydrolysed. Moreover, an increase in absorbance at 220 nm and 290 nm was also observed, which was consistent with the formation of *endo*-anhydride **3** and *p*-methoxyaniline, respectively.

The pH of the solution in the cell at completion of reaction was later raised to 11.8 by adding KOH solution (0.01 mol L^{-1}) to the cell content; this was aimed to observe any ring-opening reaction from imide that might have been formed. The UV spectrum showed no sign of absorbance change, which is indicative of either no imide having been formed, or the imide reaction was too fast to be observed at this pH. To check for this, the pH was lowered again to 6.8 by adding H_2PO_4^- solution to the cell content. It was expected to see no change in the absorbance, but when this solution was monitored again by repetitive UV scanning, it showed the same reaction observed previously for amide hydrolysis. This is indicative of amide formation from imide at pH 11.8, and the amide itself later being hydrolysed to release amine when the pH was lowered to 6.8. This suggests that the solution at pH 6.4 must have had some imide present along with anhydride and amine. The imide was either formed from amide

at pH 6.4 (along with hydrolysis reaction), or there was possibly some imide present in the prepared amide, in which the imide was unreacted until the pH was raised to 11.8 when it reacted to give amide.

The pH was raised again to 10.4 by adding KOH to the cell solution to try to detect the imide opening reaction. The UV spectrum did not show any sign of absorbance change, suggesting that there was no imide left for reaction at this stage, or the imide reaction was too fast or too slow to be detected.

2.3.3 Synthesis of imide **10**

At this stage syntheses of pure acid-amide had not been successful, so an attempt to prepare an imide **10** (Figure 2-9) was made.

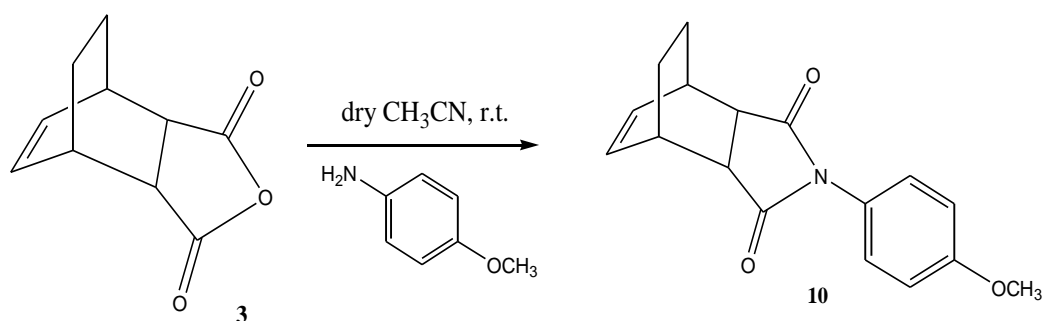


Figure 2-9: Synthesis of imide 10

The intention was that this imide, once synthesised and purified, could be converted to its acid-amide analogue by placing it in an alkaline solution in which the imide opens up to give the corresponding acid-amide as its carboxylate salt (Figure 2-10).

The reaction carried out in dry acetonitrile over 16 hours gave a 74% yield of imide.

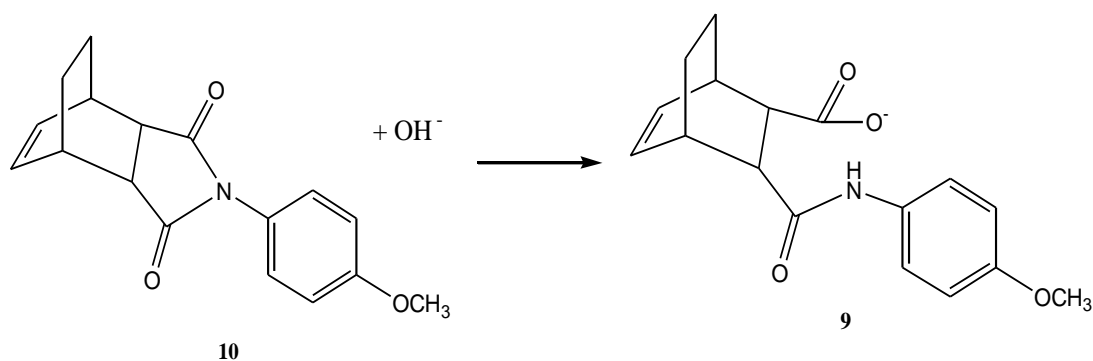


Figure 2-10: Conversion of imide to corresponding acid-amide 9

The reaction of purified **10** was studied in 0.002 mol L⁻¹ KOH solution which was monitored by repetitive UV scanning to completion. The spectrum showed an absorbance increase at 250 nm and gave an isosbestic point at 232 nm, which were indicative of formation of amide from the imide **10**.

At completion of the reaction, the pH of the cell solution was raised to a higher pH (exact pH not measured) by adding a few drops of 0.01 mol L⁻¹ KOH solution to it. The UV spectrum suggested that more amide was formed from imide as the absorbance at 250 nm was further increased and the spectrum gave the same isosbestic point at 232 nm. This suggested that the reaction is in equilibrium which is dependent on the hydroxide concentration.

This was again confirmed when the pH of the cell solution was afterwards lowered to 10.9 by adding phosphate buffer solution. The reversal of amide to imide was observed as the absorbance was decreasing at 250 nm and the UV spectrum gave the same expected isosbestic point at 232 nm. This is consistent with the compound prepared being the desired imide **10**, which gave rise to amide at high pH.

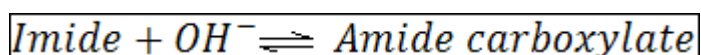
The identity of imide **10** was also later confirmed by IR and NMR spectroscopies. The NMR spectrum of imide **10** is shown in Appendix B.

2.4 Kinetic Studies of reversible ring-opening of imide 10

2.4.1 Rate constants for forward and reverse reactions

In this study the synthesised imide **10** was placed in alkaline solution which caused the imide ring to open up to give acid-amide as the carboxylate **9** (Figure 2-10).

The reaction studied was:



Therefore:

$$\text{Rate forward} = k_f [\text{imide}] [\text{OH}^-]$$

Rate reverse = k_r [amide carboxylate] (assuming it is a first order reaction with no effect from $[\text{OH}^-]$), where k_f is the second order rate constant of forward reaction, and k_r is the first order rate constant of reverse reaction.

The observed rate constant, k_{obs} , of a reaction in such an equilibrium is the sum of forward and reverse rate constants³², ie. at any fixed $[\text{OH}^-]$:

$$k_{\text{obs}} = k_f [\text{OH}^-] + k_r$$

In the current study, a number of reactions over a range of $[\text{OH}^-]$ were monitored and first order rate constants, k_{obs} , were obtained. By plotting the graph of k_{obs} versus $[\text{OH}^-]$ (Figure 2-11), k_f and k_r were determined experimentally from the gradient and y-intercept, respectively, of the apparent linear graph.

Table 2-1: k_{obs} values obtained at various $[\text{OH}^-]$

$[\text{OH}^-]$ (mol L ⁻¹)	k (min ⁻¹)
0.0200	1.47
0.0160	1.26
0.0120	0.988
0.0100	0.814
0.0080	0.561
0.0060	0.461
0.0040	0.348

The percentage errors of k_{obs} (approximately 10%) were estimated manually by plotting the maximum and minimum slope – determined from the errors of A_t and A_∞ values (each ± 0.002) – on the graphs of $\log_{10}(A_\infty - A_t)$ against t . One of these graphs is shown in Appendix C.

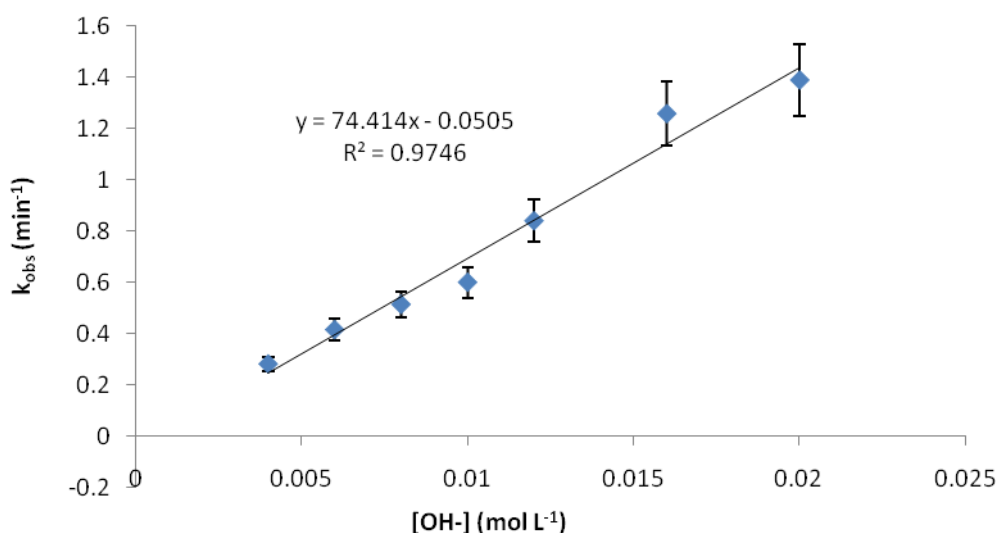


Figure 2-11: Graph of k_{obs} against $[\text{OH}^-]$

Therefore, it could be determined from the plot that k_f (conversion of imide to amide carboxylate) was $74 \pm 16 \text{ L mol}^{-1} \text{ min}^{-1}$. The error was estimated from the error of slope (Appendix C). The intercept is a negative value (-0.05 min^{-1}) but the experimental error from extrapolation is large ($\pm 0.12 \text{ min}^{-1}$), so more investigations would be needed to determine the value of intercept (k_r) if it is non-zero.

All of the above calculations are based on an assumption that the reverse reaction is pH-independent: $k_{\text{obs}} = k_f [\text{OH}^-] + k_r$.

However, if the reverse reaction was somehow also dependent on $[\text{OH}^-]$, then:

$$\begin{aligned} k_{\text{obs}} &= k_f [\text{OH}^-] + k_r [\text{OH}^-] \\ &= (k_f + k_r) [\text{OH}^-] \end{aligned}$$

This would end up giving a linear plot through the origin and this cannot be excluded from the data in Figure 2-11.

But, since the equilibrium constant is given by the ratio of forward to back reaction rate constants, it would in this case be given by:

$$K = \frac{k_f[\text{OH}^-]}{k_r[\text{OH}^-]} = \frac{k_f}{k_r}.$$

This requires that the position of equilibrium is independent of hydroxide concentration, but this is inconsistent with earlier observations (section 2.3.3) that the extent of reaction of imide increased with increasing pH.

A third possibility is that the reverse amide carboxylate to imide reaction has two terms, one first order, the other second order in $[\text{OH}^-]$:

Rate of reverse reaction = $k_r(1)$ [amide carboxylate] + $k_r(2)$ [amide carboxylate] $[\text{OH}^-]$, whereby:

$$\begin{aligned}k_{\text{obs}} &= k_f [\text{OH}^-] + k_r(1) + k_r(2)[\text{OH}^-] \\ &= (k_f + k_r(2)) [\text{OH}^-] + k_r(1)\end{aligned}$$

This would give a non-zero intercept but the gradient would now represent the sum of k_f and $k_r(2)$.

Irrespective of whether the ring opening process of imide **10** in this study is of any of the three cases, the pH-dependence of the reverse imide-formation reaction itself needs to be studied independently with the amide carboxylate as reactant at lower pH, where $[\text{OH}^-]$ is too low to promote the forward imide opening reaction. If the reverse reaction is independent of $[\text{OH}^-]$ then only the first of the above three cases would be consistent.

2.4.2 Equilibrium Constant, K

An accurately determined value of the rate constant for the reverse imide-forming reaction of amide carboxylate would also allow calculation of an accurate value for the equilibrium constant, K, using the value for k_f from section 2.4.1.

The other way to independently determine the value of K is from absorbance changes rather than rates. K could be calculated from the final absorbance (A) values of the individual runs at different hydroxide concentrations as the following analysis shows.

If:

A_i = Initial absorbance at zero (mixing) time;

A_t = Absorbance at end of reaction for that particular $[OH^-]$;

A_∞ = Absorbance for complete conversion to amide as would occur at very high $[OH^-]$.

And if:

$$\Delta A_t = A_t - A_i;$$

$$\Delta A_\infty = A_\infty - A_i.$$

Then:

ΔA_t is directly proportional to the amount of amide formed for this $[OH^-]$;

ΔA_∞ is directly proportional to 100% conversion of imide to acid-amide;

$$\therefore \frac{\Delta A_t}{\Delta A_\infty} = \text{fraction of the amide conversion at certain hydroxide}$$

concentration;

$(\Delta A_\infty - \Delta A_t)$ is directly proportional to the amount of amide that is yet to form, i.e. directly proportional to the amount of imide.

Therefore, assuming again that the reaction is independent of $[OH^-]$ in the reverse directions:

$$K = \frac{[Product]}{[Reactant]} = \frac{[amide]}{[imide][OH^-]} = \frac{\Delta A_t}{(\Delta A_\infty - \Delta A_t)[OH^-]}$$

By rearranging the formula:

$$\frac{1}{\Delta A_t} = \left(\frac{1}{K} \times \frac{1}{\Delta A_\infty} \right) \frac{1}{[OH^-]} + \frac{1}{\Delta A_\infty}$$

Therefore, by plotting $\frac{1}{\Delta A_t}$ versus $\frac{1}{[OH^-]}$, the equilibrium constant, K, can

be calculated from the values obtained from the y-intercept and gradient of the linear graph. This would allow the equilibrium constant to be determined without taking amide conversion to completion in case there are some unavoidable experimental errors (e.g. not knowing at which hydroxide concentration the amide conversion is complete).

It was intended to apply this analysis once it had been developed in principle to the kinetic runs at varying $[OH^-]$ but the reactions had been so fast in relation to the time taken to mix solutions and take early absorbance readings that extrapolation of first-order kinetic analysis plots to zero (mixing) time was too inaccurate to give reliable zero time absorbance values. Plots based on the above linear relationship were subject to too large error to be useful. Probably better data could have been obtained for this purpose at lower $[OH^-]$ for which the extrapolation to zero time A would have been more reliable but insufficient time prevented this additional study. In any case, accurate values for k_r as determined in the next section using amide carboxylate as reactant allowed an accurate value for K to be established.

2.5 Kinetic studies towards acid-amide 9 using buffer solutions

2.5.1 Introduction

Since it has been shown that acid-amide **9** can be successfully obtained from imide **10**, the pH-rate profile of the reaction of **9** can thus be established by reacting **9** at different lower pH values.

We are primarily interested in the potential of the drug model system to release amine (i.e. hydrolysis reaction) more rapidly at pH 6.5 (tumour tissues environment) than at pH 7.4 (normal tissues environment). In the pH region of primary interest, both the ionised and neutral forms of acid-

amide will be present (in proportions differing with pH). Thence a kinetic analysis is required to obtain rate constants for the reaction of both species, of which the products would need to be determined alongside the kinetic analysis.

It is already known from the previous sections that the ionised amide gives only the imide product; it does not hydrolyse as the amide solution at high pH is quite stable. Ideally for prodrug application the neutral acid-amide would give hydrolysis only, and earlier studies with related systems^{33, 34} suggest this may be so, but a check that the acid-amide in neutral form gives no imide as well would be helpful in assessing its prodrug potential.

From kinetic analysis of the higher pH (given by hydroxide solutions) study on imide opening to amide, a rate constant for the reverse amide \rightarrow imide reaction might have been obtained (**section 2.4**) but the experimental error was too large. A value is needed through direct study at a lower pH range of 9-10 where the acid-amide remains fully ionised but where $[\text{OH}^-]$ is too low for significant ring opening of imide to occur. This study is covered in section 2.5.2. The obtained rate constant would contribute to overall k_{obs} down in pH until the acid-amide is fully in neutral form.

The reaction of the neutral form of acid-amide would contribute to the overall k_{obs} which is suspected to increase with decreasing pH as more neutral form is present. At sufficiently low pH, the acid-amide will be in fully neutral form and further reduction in pH will have no effect on the rate and rate constant. If the reaction is not too fast to be measured at this low pH, a plateau should be reached in the pH-rate profile from which the limiting rate constant, k_{lim} , can be obtained directly, but if the reaction is too fast the data may still be analysed to obtain k_{lim} and pK_a . This is covered in section 2.5.3.

2.5.2 pH rate profile of ionised acid-amide

The kinetic analysis of ionised acid-amide was conducted to confirm the rate constant for the reformation of imide from amide which was determined in section 2.4. This was done at a lower pH range (pH 9-10) by means of a series of carbonate buffer solutions.

The kinetic analysis was conducted on a Hewlett Packard Agilent 8453 UV/Vis spectrophotometer. The acid-amide **9** was prepared in solution by adding imide **10** to 0.1 mol L⁻¹ KOH solution. Samples were then added to various carbonate buffer solutions at 30.0°C and the k_{obs} values and their standard deviations (sd) were calculated, by the Agilent Chemstation software, using the absorbance values obtained at 247 nm (λ_{max} of acid-amide).

The k_{obs} values across the pH range of 9-10 were apparently constant within experimental error (Table 2-2) and it appears that these rate constant values are independent of the hydroxide concentrations. The average k_{obs} value was calculated to be $0.067 \pm 0.011 \text{ min}^{-1}$. This indicates that the y-intercept value ($-0.05 \pm 0.12 \text{ min}^{-1}$) from Figure 2-11 is actually a positive value, hidden by the large experimental error.

Table 2-2: k_{obs} values obtained within the pH range of 9-10

pH	k_{obs} (min^{-1})	standard deviation (min^{-1})
9.91	0.074	0.005
9.43	0.065	0.005
9.34	0.064	0.002
9.32	0.062	0.005
9.06	0.071	0.011

From section 2.5.3 below similar values for k_{obs} were obtained using malonate buffer solutions at the lower pH 7.5-8.5, indicating that the protonation of hydrolysable neutral acid-amide is negligible at this pH range as well.

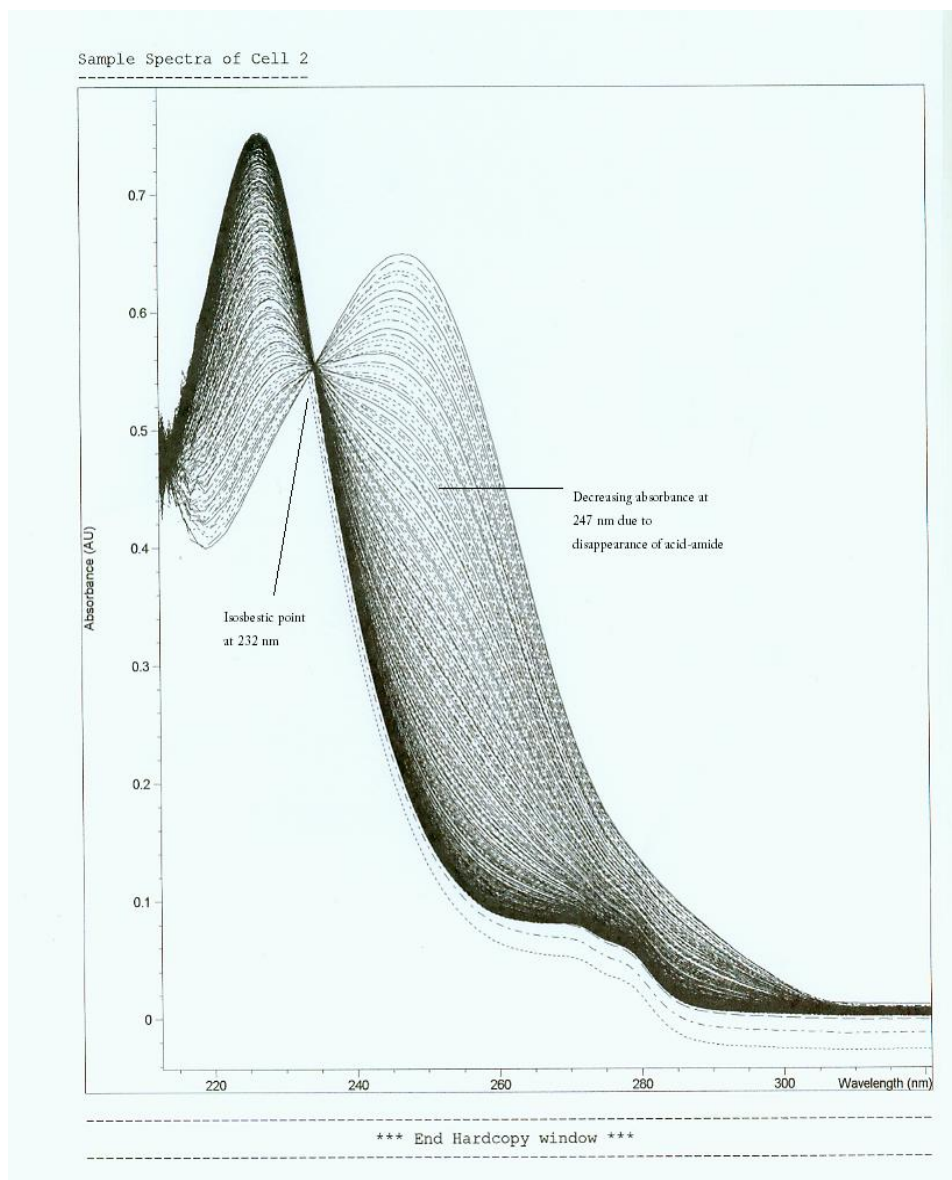


Figure 2-12: An example of the UV/Vis repetitive scanning spectrum of 1:1 carbonate buffer (pH 9.43)

A previous study on an imide ring-opening equilibrium promoted by OH^- was carried out by Shafer *et al.* on *N*-methylphthalimide²³ (Figure 2-13). This was carried out at 37°C and ionic strength, μ , of 0.2. A plot of k_{obs} versus $[\text{OH}^-]$ gave k_f , from the slope of the plot, as approximately 1800 $\text{L mol}^{-1} \text{min}^{-1}$, which was considerably higher than the k_f value calculated in the current study as 74 $\text{L mol}^{-1} \text{min}^{-1}$. That is, imide **10** is much more stable to ring-opening than the aromatic imide reported by Shafer *et al.*

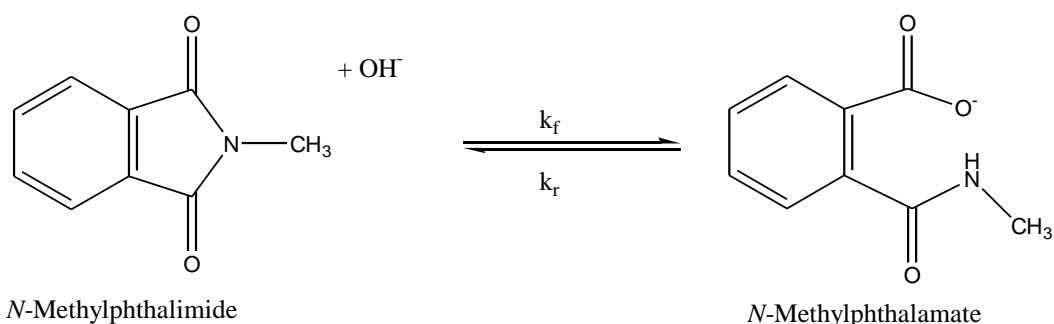


Figure 2-13: Imide ring-opening equilibrium reaction studied by Shafer *et al.*²³

The equilibrium constant ($K = k_f/k_r$) for ring-opening is correspondingly much higher for the aromatic imide. Shafer *et al.* reported a K value of $4 \times 10^7 \text{ L mol}^{-1}$. In contrast, from the current study the K was calculated to be only 1100 L mol^{-1} . The value of k_r (0.067 min^{-1}) for imide **10** is about 15 times larger at 30°C than that for the aromatic imide (0.0045 min^{-1}) at 37°C . These differences suggest that the aromatic imide is much more prone to ring-opening and less to ring closure, reflecting perhaps greater strain in the ring-closed system in which the aromatic ring-fused bond is shortened compared to the aliphatic bond in the current molecule.

Ring-closure to form anhydride as part of the hydrolysis reaction at lower pH (see section 2.5.3) may equally be faster for the aliphatic systems, which would enhance their potential as anti-cancer prodrugs.

However, the *N*-substituent differs between the two molecules (methyl versus *p*-methoxyphenyl) and there are doubtless contributions to the differences resulting from electronic effects on rates and equilibrium position.

2.5.3 pH rate profile incorporating neutral acid-amide

The acid-amide **9** solution prepared in 0.1 mol^{-1} KOH as described in section 2.5.2 was reacted in the following buffer solutions at 30.0°C :

- Phosphate buffer – pH range: 5.5-7.5
- Malonate buffer (second ionisation) – pH range: 4.5-8.5
- Malonate buffer (first ionisation) – pH range: 2-4

The k_{obs} values and their standard deviations were again calculated by the Agilent Chemstation software, and a graph of k_{obs} against pH was then plotted to obtain the pH-rate profile of the acid-amide.

Table 2-3: k_{obs} values obtained at various pH

pH	k_{obs} (min^{-1})	pH	k_{obs} (min^{-1})
2.33	0.5368	5.90	0.1253
2.77	0.5068	6.02	0.1126
3.21	0.4576	6.10	0.1042
3.44	0.4311	6.45	0.0926
3.64	0.4213	7.06	0.0722
3.86	0.4122	7.49	0.0647
4.65	0.3395	8.11	0.0713
4.82	0.3103	9.06	0.0710
5.32	0.2231	9.32	0.0619
5.59	0.1724	9.34	0.0642
5.67	0.1613	9.43	0.0644
5.84	0.1306	9.91	0.0742

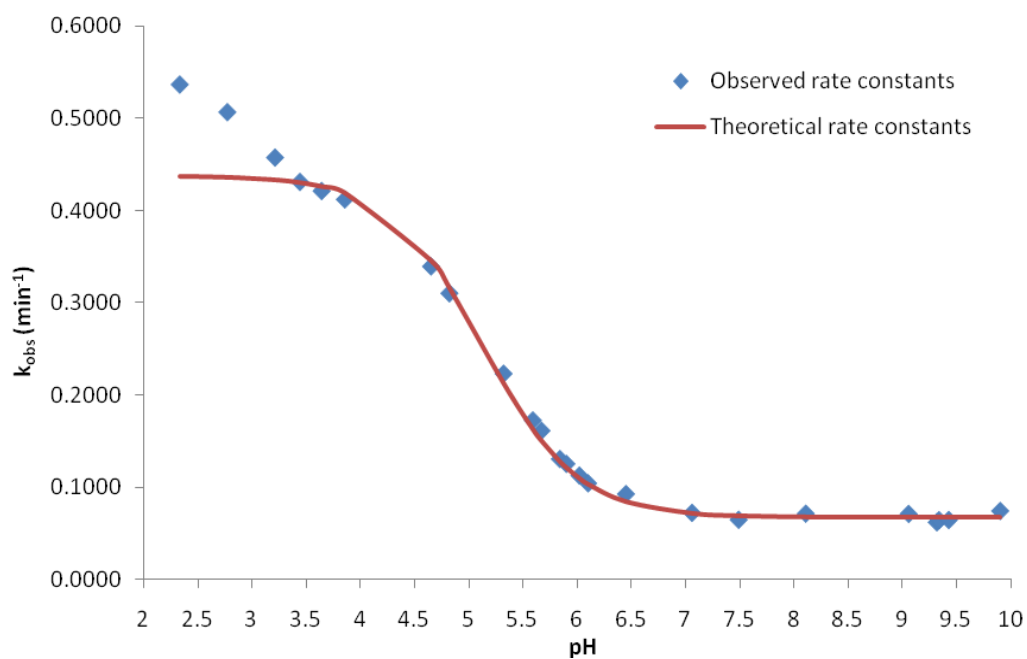


Figure 2-14: pH rate profile established for acid-amide 9 [30.0°C, μ 1.00 (KCl)]. The best fit line is based on equation (7) (see later).

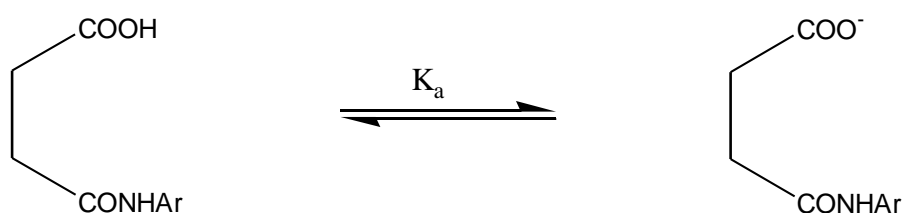
The rate data within the pH 3-7.5 range were analysed according to a modified form of the following equation derived by Menger and Ladika²¹

$$\frac{1}{k_{obs}} = \frac{K_a}{k_{lim}[H^+]} + \frac{1}{k_{lim}}$$

where K_a is the carboxyl ionisation constant, and k_{lim} is the limiting rate constant at 100% conjugate acid.

The modification was needed to take account of the contribution to rate of higher pH reaction of amide carboxylate to form imide.

For the equilibration of acid-amide and its amide carboxylate anion:



Let this fraction = f
(may either hydrolyse
or form imide)

Let this fraction = $1-f$
(can only form imide)

If k_{lim} is the lower pH plateau rate constant (100% of neutral acid-amide, excluding any $[H^+]$ catalysis), and k_{low} is the higher pH plateau rate constant for amide carboxylate (can only form imide), then:

$$\begin{aligned} k_{obs} &= f k_{lim} + (1 - f) k_{low} \\ &= f(k_{lim} - k_{low}) + k_{low} \quad \text{--- (1)} \end{aligned}$$

$$\therefore (k_{obs} - k_{low}) = f(k_{lim} - k_{low}) \quad \text{--- (2)}$$

$$f = \frac{[RCOOH]}{([RCOOH] + [RCOO^-])}$$

$$\frac{1}{f} = \frac{[RCOOH] + [RCOO^-]}{[RCOOH]}$$

$$= 1 + \frac{[RCOO^-]}{[RCOOH]} \text{----- (3)}$$

$$K_a = \frac{[RCOO^-][H^+]}{[RCOOH]}$$

$$\therefore \frac{K_a}{[H^+]} = \frac{[RCOO^-]}{[RCOOH]} \text{----- (4)}$$

Substituting (4) into (3):

$$\frac{1}{f} = 1 + \frac{K_a}{[H^+]} \text{----- (5)}$$

By inverting (2):

$$\frac{1}{(k_{obs} - k_{low})} = \left(\frac{1}{f}\right) \left(\frac{1}{(k_{lim} - k_{low})}\right) \text{----- (6)}$$

Substituting (5) into (6):

$$\begin{aligned} \frac{1}{(k_{obs} - k_{low})} &= \left(1 + \frac{K_a}{[H^+]}\right) \left(\frac{1}{(k_{lim} - k_{low})}\right) \\ &= \frac{1}{k_{lim} - k_{low}} + \left(\frac{K_a}{(k_{lim} - k_{low})} \times \frac{1}{[H^+]}\right) \end{aligned}$$

$$\therefore \frac{1}{(k_{obs} - k_{low})} = \frac{K_a}{(k_{lim} - k_{low})} \left(\frac{1}{[H^+]}\right) + \frac{1}{(k_{lim} - k_{low})} \text{----- (7)}$$

This requires an independently (higher pH) calculated value for k_{low} (taken to be 0.067 min^{-1} , see section 2.5.2), whereby k_{lim} can be obtained from the intercept and thereby, K_a from the gradient of a plot of $1/(k_{obs} - k_{low})$ against $1/[H^+]$.

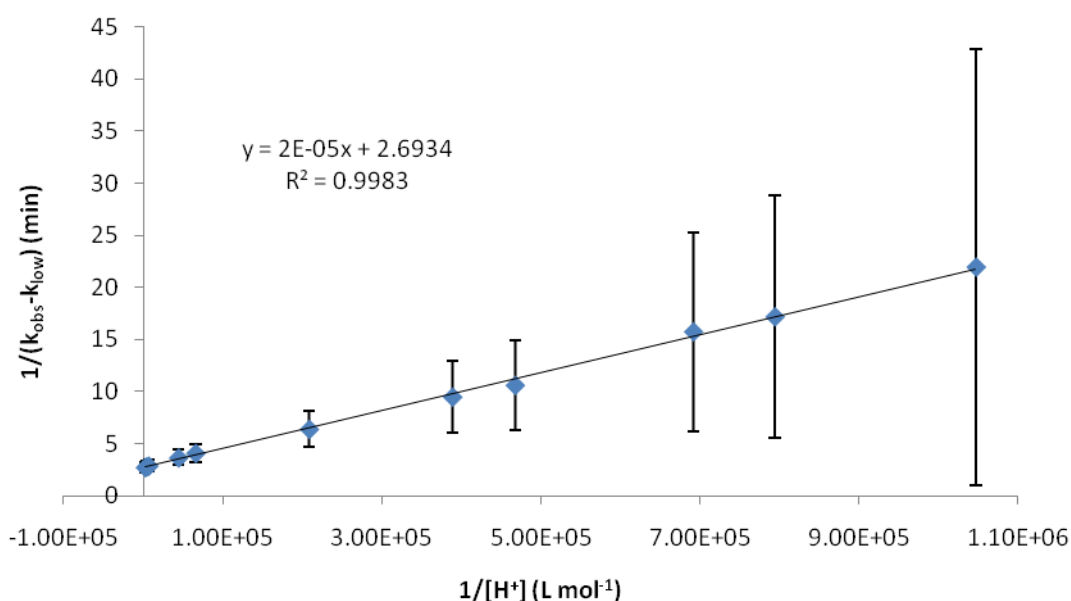


Figure 2-15: Graph of $1/(k_{\text{obs}}-k_{\text{low}})$ vs $1/[H^+]$

Applying this to the current data, the straight line graph (Figure 2-15) allows the values of k_{lim} and pK_a to be calculated, which turned out to be $0.44 \pm 0.03 \text{ min}^{-1}$ and 5.1 ± 0.4 , respectively. These values when applied to equation (7) provide the calculated line of best fit in Figure 2-14. The deviation at low pH, which is outside the range of interest for prodrugs, may be a result of H^+ catalysis but time limitation has prevented further study on this.

The errors estimations for k_{lim} and pK_a values are showed in appendix D.

Proof that the low pH reaction of neutral acid-amide is hydrolysis only and not imide formation was obtained by carrying out a one-off reaction of acid-amide in buffered malonate solution at pH 3.9, monitoring reaction to completion, then raising pH to 11.1 by addition of a calculated amount of K_3PO_4 to reference and sample cells. At this pH, the rate of ring-opening of any imide present would have a half-life of about 10 minutes, and the equilibrium constant for the reaction is around 1 from the data in sections 2.4.1 and 2.4.2. Therefore a rapid reaction of around 50% of any imide present would be easily detected by increased absorbance at 247 nm (λ_{max} for acid-amide). No change was observed over 18 hours, indicating that the neutral acid-amide gives hydrolysis only.

In the current study, acid-amide **9** was prepared as an analogue of Glüsenkamp's acid-amide **9b** (Figure 1-6). Glüsenkamp *et al.*²² reported a pK_a value of 5.9 and an extraordinarily high k_{lim} value of 6.93 min^{-1} . This was carried out at 37°C and 150 mM salt concentration. These values were considerably higher than the acid-amide **9** of the current study, of which the pK_a and k_{lim} values were determined to be 5.13 and 0.44 min^{-1} respectively. Glüsenkamp's acid-amide was however a tertiary aliphatic one and this would be expected to influence rate significantly even if not to pK_a .

Kluger and Lam³⁴, on the other hand, also reported a similar acid-amide molecule, differing only in having a 1-carbon bridge at C-1,4 positions (Figure 2-16), in contrast to a 2-carbon bridge for the current acid-amide **9** molecule (Figure 3-4).

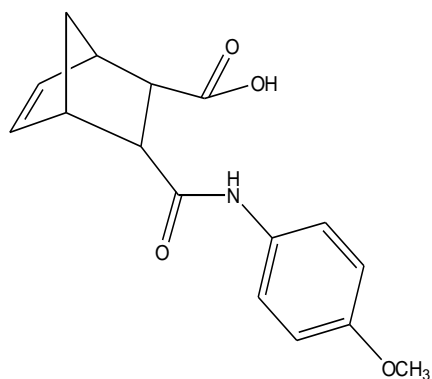


Figure 2-16: Kluger's acid-amide³⁴

The hydrolysis reaction of the above compound was carried out at an ionic strength of 1.0 with KCl, and at a temperature of 50°C . Kluger and Lam reported that the hydrolysis reaction gave a pK_a value of 5.0 and a hydrolysis rate of 0.87 min^{-1} . The acid-amide **9** in the current study shows a pK_a very similar to Kluger's and the rate of reaction of the neutral acid-amide at 30.0°C is about half that of Kluger's at 50°C . Direct comparison is not possible but the increased bridge size in the molecule does not appear to have a significant effect on either pK_a or rate, even if the results from the study by Glüsenkamp suggest a high sensitivity of both pK_a and rate to minor structural changes.

3 Materials and Methods

3.1 Materials

Dry solvents

Specifically dry solvents including diethyl ether, tetrahydrofuran (THF) and dichloromethane were obtained from the solvent purification system.

Nitrogen-saturated, CO₂-free distilled water

This was used for all preparations of buffer solutions used for kinetic analyses. Distilled water was boiled for at least 3 hours, after which it was cooled to room temperature while being gently flushed with nitrogen gas. Once it was cold and saturated with nitrogen a drying tube with CO₂-adsorbent was attached to the flask to keep the water free of CO₂.

3.2 General methods

NMR Spectroscopy

All ¹H NMR spectral work was performed on either Brüker DRX 300 FT-NMR (300 MHz) or Brüker DRX 400 FT-NMR (400 MHz) spectrometers with deuterated chloroform or deuterated acetone as the solvents. Chemical shifts are expressed in parts per million (ppm) and are given in δ. ¹H chemical shifts for the deuterated solvents are referenced as follows: CDCl₃ - 7.24 ppm; (CD₃)₂C=O - 2.04 ppm. Spin multiplicities are indicated by the following symbols: *s* (singlet); *d* (doublet), *t* (triplet), *m* (multiplet), *dd* (doublet of doublets).

Infrared Spectroscopy

All infrared (IR) spectra were recorded on a Perkin-Elmer Spectrum 100 FT-IR spectrophotometer over the range of 4500 – 450 cm⁻¹ at 1 cm⁻¹ resolution. Samples were either prepared as a KBr disc or run neat between two polished KBr discs.

Ultraviolet/Visible Spectroscopy

All UV/Vis studies were conducted either on a Kontron UVIKON 860 spectrophotometer (wavelength range 180-900 nm) or Hewlett-Packard 8453 Diode Array spectrophotometer (wavelength range 180-900 nm) coupled with the Agilent Chemstation software for kinetic analyses.

Melting points

Melting points were measured, uncorrected, using a Reichert thermopan melting point apparatus.

pH Measurements

pH measurements were done on Radiometer pHM 240 using a Schott Gerate H6180 electrode.

Elemental analysis

An elemental analysis of imide **10** was performed at the Campbell Microanalytical Laboratory, University of Otago, Dunedin, New Zealand.

3.3 Preparation of compounds

3.3.1 *endo*-Bicyclo[2.2.2]octa-5-ene-2,3-dicarboxylic anhydride **3**

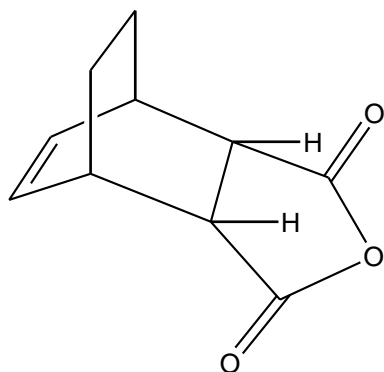


Figure 3-1: *endo*-Bicyclo[2.2.2]octa-5-ene-2,3-dicarboxylic anhydride **3**

This method was adapted from Birney *et al.*²⁸. To maleic anhydride (**2**; 1.058 g, 10.8 mmol) was added chloroform (25 mL). The solution was cooled with ice and to this was slowly added 1,3-cyclohexadiene (**1**; 1.03

mL, 11 mmol). The solution was let warm to room temperature and to react overnight in the dark. The chloroform was then removed *in vacuo*, the residue was recrystallised from dichloromethane, collected and dried overnight to yield white needle-like crystals (0.681 g, 35%) of *endo*-bicyclo[2.2.2]octa-5-ene-2,3-dicarboxylic anhydride **3**. M.p. 147°C (lit.³⁵ 147°C); IR (in CH₂Cl₂): 1781 cm⁻¹ (anhydride C=O).

3.3.2 Attempted synthesis of amide ester 7

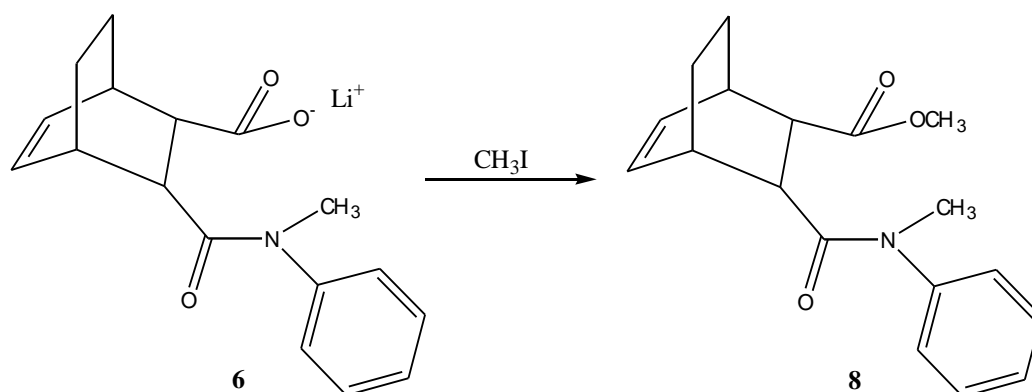


Figure 3-2: Acid-amide salt **6** was prepared, and this was used in an attempt to synthesise the amide ester **8**.

The acid-amide salt **6** was first prepared. The method was a repetition of the synthesis carried out for directed-study research²⁴. The reaction was carried out in a flask in a chlorobenzene slush bath cooled with liquid nitrogen, with nitrogen gas flowing through the reaction flask. In a 3-neck 250 mL round bottom flask, *N*-methylaniline **4** (in 2 mol L⁻¹ cyclopentane; 0.18 mL, 1.69 mmol) was dissolved in dry ether (10 mL). Butyllithium (0.85 mL, 1.69 mmol) was later added drop wise with stirring to form the lithium amide. Meanwhile, *endo*-anhydride **3** (0.301 g, 1.69 mmol) was dissolved, in a flask heated with warm water, in dry ether (20 mL), and to this the lithium amide solution was slowly added with stirring. The reaction mixture was left for 2 hours, after which the slush bath was removed and the reaction vessel was left at room temperature overnight in the dark to give the ionised acid-amide salt **6**.

Ether was later removed *in vacuo*. The dry residue was dissolved in acetone (pre-dried with 4 Å molecular sieves), and to this was added methyl iodide (0.50 mL; 10 times excess). Oven-dried potassium carbonate (K_2CO_3 ; 0.117 g, 0.5 mol equiv.) was later added to the solution with stirring, and the reaction was monitored by TLC (25% ether/hexane). IR (in CH_2Cl_2): 1782 cm^{-1} (anhydride C=O); 1635 cm^{-1} (amide C=O), 1595 cm^{-1} (aromatic and aliphatic C=C).

The solids were filtered, and acetone was removed *in vacuo* to leave the product in solid form for analyses.

The IR samples were prepared by dissolving a small amount of product in minimal amount of dichloromethane, which was then transferred to a KBr cell and analysed. The IR spectrum showed a strong peak at 1635 cm^{-1} , indicating the presence of an amide group. However, a weak peak of residual anhydride at 1782 cm^{-1} was also observed and there was no sign of an ester carbonyl stretch ($1730\text{-}1750\text{ cm}^{-1}$).

NMR samples were prepared by dissolving a small amount of product in $CDCl_3$. The NMR spectrum also could not confirm the formation of amide ester **8** as the peak of amide methyl proton ($C(O)NCH_3$) was not found on the spectrum.

The attempted synthesis of **8** was repeated using a different solvent dimethylformamide (DMF) with heating for the attempted methylation reaction. However, the TLC analysis again showed no sign of product formation.

3.3.3 Attempted direct synthesis of acid-amide 7

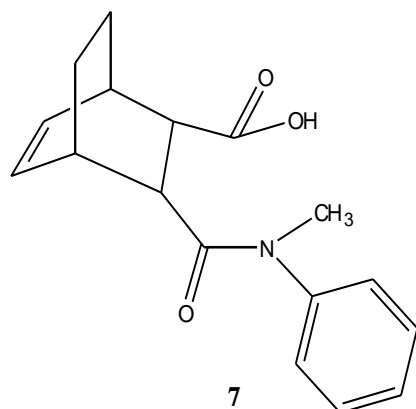


Figure 3-3: Acid-amide 7

endo-Anhydride **3** (0.102 g, 0.57 mmol) was dissolved in peroxide-free 1,4-dioxane (5 mL, treated by activated alumina (Brockmann, Grade II)), and to this was added quickly *N*-methylaniline (0.06 mL, 0.57 mmol). An extra 10 mL of 1,4-dioxane was added before the mixture was left to reflux overnight, and the reaction was monitored by TLC (20% ethyl acetate/diethyl ether).

No reaction was observed from the TLC plate, thus dimethylaminopyridine (DMAP, 0.007 g, 0.057 mmol) was added to the solution and the reaction was continued and monitored by TLC. After an overnight reaction, the TLC showed no formation of product.

3.3.4 Attempted synthesis of acid-amide 9

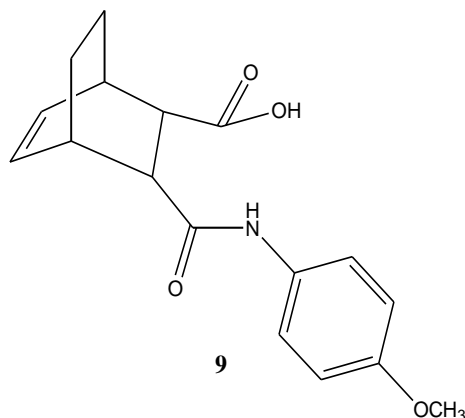


Figure 3-4: Acid-amide 9

p-Methoxyaniline (or more commonly known as *p*-anisidine) is toxic and can cause blood damage upon oral ingestion, inhalation or skin contact. If heated strongly, it may release very toxic fumes of nitrogen oxides³⁶. Prior to use, it was purified by recrystallising from activated charcoal.

p-Methoxyaniline (0.213 g, 1.73 mmol) and *endo*-anhydride (0.308 g, 1.73 mmol) were dissolved in dry ether in separate flasks (*endo*-anhydride was first dissolved with heating) before the two were combined together. Precipitate was immediately formed, but the reaction was left overnight with stirring and monitored by TLC (20% ethyl acetate/diethyl ether), until the disappearance of reactant was observed on the TLC plate. The precipitated solid was filtered, dried *in vacuo*, and later recrystallised from ether/CH₂Cl₂ mixture solution to yield crude **9** (0.190 g, 36%). M.p. 138°C. IR (in CH₂Cl₂): 1780 cm⁻¹ (anhydride C=O), 1731 cm⁻¹ carboxylic acid C=O), 1649 cm⁻¹ (amide C=O).

Even though the amide peak was observed, the IR spectrum still showed an anhydride peak at 1780 cm⁻¹, suggesting the impurity of **9** even after the recrystallisation reaction.

3.3.5 Synthesis of imide 10

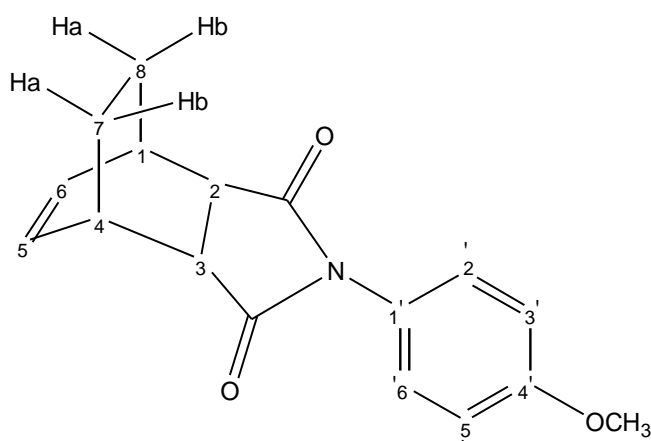


Figure 3-5: Imide 10

This method was adapted from Billett *et al*³¹. *endo-Anhydride 3* (0.501 g, 2.81 mmol) and *p*-methoxyaniline (0.347 g, 2.81 mmol) were dissolved separately in dry acetonitrile before the two were combined. The synthesis of imide **10** was then carried out under reflux at 80°C overnight using an oil bath, and the reaction was monitored by TLC (25% ethyl acetate/diethyl ether) until the product formation seemed to have completed. The solvent was removed *in vacuo* and the product was recrystallised from ethanol to give imide **10** as white fluffy crystals (0.593 g, 74%), m.p. 158-161°C; Anal. Calc. for C₁₇H₁₇NO₃: C, 72.06; H, 6.05; N, 4.94. Found: C, 72.30; H, 6.27; N, 4.98%. IR (KBr in CH₃CN): 1777 cm⁻¹ (imide C=O), 1709 cm⁻¹ (imide C=O). ¹H NMR (400.13 MHz) (CDCl₃): δ 1.44 (*m*, 2H, H-7a,8a or H7b,8b), 1.63 (*m*, 2H, H7a,8a or H7b,8b), 2.98 (*m*, 2H, H1,4), 3.24 (*m* (br), 2H, H2,3), 3.81 (*m*, 3H, OCH₃), 6.29 (*dd*, 2H, H5,6), 6.93-6.95 (*dd*, 2H, H2',6'), 7.07-7.10 (*dd*, 2H, H3',5').

3.4 Solutions preparation for kinetic studies of ring-opening of imide 10

During the conversion of imide **10** to acid-amide **9** (Figure 2-10), OH⁻ is consumed but only at a ratio of one mole per every mole of imide. Therefore at the low concentrations of imide (ca. 7x10⁻⁵ mol L⁻¹) in the reaction solutions monitored for kinetics, this would have a negligible effect on the concentration of OH⁻ (0.004-0.020 mol L⁻¹).

The following solutions were prepared:

- 1.00 mol L⁻¹ potassium chloride (KCl) solution
- Standardised 0.10 mol L⁻¹ potassium hydroxide (KOH) in 0.90 mol L⁻¹ KCl solution 9 (overall ionic strength 1.00)
- 0.0035 mol L⁻¹ imide stock solution in THF

The kinetic studies of imide ring opening reaction at hydroxide concentration of 0.020 mol L⁻¹ were carried out by adding the imide (50 µL) into the KCl solution (2 mL) in a quartz cell cuvette. This was placed in the thermostated cell block of the UVIKON spectrophotometer at 30.0°C and

was referenced against an identical solution in a reference cell. The reaction was started by adding KOH solution (0.50 mL, pre-equilibrated at 30.0°C) to the cell solution in advance to the reference cell. The absorbance values were recorded at 247 nm (λ_{\max} of acid-amide³⁷) at pre-set time intervals (0.2 minutes) and integration time (0.7 seconds) for 40-50 cycles until the reaction reached its infinity state.

The experiment was repeated similarly at different hydroxide concentrations (0.004-0.020 mol L⁻¹; refer to the following table), while the time intervals and λ_{\max} were kept constant.

Table 3-1: Preparation of solutions for kinetic runs

Total Hydroxide concentration [OH ⁻] (mol L ⁻¹)	1.0 mol L ⁻¹ KCl solution (mL)	Imide stock solution (mL)	0.10 mol L ⁻¹ KOH / 0.90 mol L ⁻¹ KCl solution (mL)
0.0200	2.00	0.050	0.50
0.0160	2.10		0.40
0.0120	2.20		0.30
0.0100	2.25		0.25
0.0080	2.30		0.20
0.0060	2.35		0.15
0.0040	2.40		0.10

3.4.1 Calculation of rate constants for forward and reverse reactions (k_r and k_f)

For each hydroxide concentration, absorbance recorded at each time interval (A_t) was subtracted from the absorbance at infinity (A_∞), and later $\log_{10}(A_\infty - A_t)$ was plotted against time. The observed rate constant (k_{obs}) was determined by multiplying the gradient of the linear graph by -2.303 (see equation (8) in section 0).

Once all the k_{obs} values were determined for every hydroxide concentration, they were plotted against $[\text{OH}^-]$ to obtain a linear graph. From this the rate constants for forward and reversed reaction (k_f and k_r respectively) could be determined (see section 2.4.1), where:

k_r = y-intercept;

k_f = gradient.

3.5 Kinetic studies of acid-amide 9 conversion using various buffer solutions

In this section all UV/Vis studies were conducted on a Hewlett-Packard Agilent 8453 Diode Array spectrophotometer

3.5.1 Introduction

An alternative of using different concentrations of potassium hydroxide solutions is to use a series of buffered solutions which avoids the need to keep the reaction conditions to be CO_2 -free. However, using buffered solutions might give some buffer reactions or catalysis. For example, for carbonate buffer solutions, CO_3^{2-} may act as base in place of OH^- to open the imide to amide, whereas HCO_3^- may act as a general acid to catalyse the reaction. Likewise for the reverse reaction, reformation of imide from amide might possibly be acid-catalysed by HCO_3^- . The catalysis problem would need to be checked by diluting the buffered solutions at constant pH (i.e. constant ratio of $\text{CO}_3^{2-}/\text{HCO}_3^-$) and ionic strength and using the diluted solutions to check for reduced rate.

The various buffer solutions for kinetic runs were prepared at constant ionic strength $\mu = 1.00$, where:

$$\mu = \frac{1}{2} \sum c_i z_i^2$$

For example, for a carbonate buffer solution made up with KHCO_3 and K_2CO_3 :

$$\mu = \frac{1}{2} \{ [K^+](1)^2 + [HCO_3^-](1)^2 + [K^+](1)^2 + [H_2CO_3^{2-}](2)^2 + [K^+](1)^2 + [Cl^-](1)^2 \}$$

where the last two terms represent $[K^+]$ and $[Cl^-]$ from 2.0 mol L^{-1} KCl solution added to bring the net ionic strength to 1.00. For other buffer solutions, KCl was routinely used to maintain ionic strength at 1.00.

3.5.2 Preparation of buffer solutions

The following solutions were prepared:

- 0.200 mol L^{-1} $KHCO_3$ solution
- 0.200 mol L^{-1} K_2CO_3 solution
- 0.200 mol L^{-1} KH_2PO_4 solution
- 0.200 mol L^{-1} K_2HPO_4 solution
- 0.200 mol L^{-1} $H(COO)_2KCH_2$ (KMal) solution
- 0.200 mol L^{-1} $(COO)_2K_2CH_2$ (K_2 Mal) solution
- 0.200 mol L^{-1} $H_2(COO)_2CH_2$ (H_2 Mal) solution
- 2.0 mol L^{-1} KCl solution

A series of carbonate, phosphate and malonate buffer solutions (all with a concentration of 0.100 mol L^{-1} and an ionic strength of 1.0) were prepared by mixing the above solutions at different ratios:

Table 3-2: Preparation of carbonate buffer solutions (pH range 9-10)

$KHCO_3/K_2CO_3$ buffer ratio	$KHCO_3$ solution (mL)	K_2CO_3 solution (mL)	KCl solution (mL)	Water (mL)
1:5	1.7	8.3	7.4	2.6
1:1	5.0	5.0	8.0	2.0
3:1	7.5	2.5	8.5	1.5
5:1	8.3	1.7	8.7	1.3
10:1	9.1	0.9	8.8	1.2

Table 3-3: Preparation of phosphate buffer solutions (pH range 5.5-7.5)

KH₂PO₄/K₂HPO₄ buffer ratio	KH₂PO₄ solution (mL)	K₂HPO₄ solution (mL)	KCl solution (mL)	Water (mL)
1:9	1.0	9.0	7.2	2.8
1:3	2.5	7.5	7.5	2.5
1:1	5.0	5.0	8.0	2.0
3:1	7.5	2.5	8.5	1.5
4:1	8.0	2.0	8.6	1.4
5:1	8.3	1.7	8.7	1.3
7:1	8.8	1.2	8.8	1.2
9:1	9	1	8.8	1.2

Table 3-4: Preparation of malonate buffer solutions (second ionisation) (pH range 4.5-8.5)

KHMal/K₂Mal buffer ratio	KHMal solution (mL)	K₂Mal solution (mL)	KCl solution (mL)	Water (mL)
1:9	1.0	9.0	7.2	2.8
1:3	2.5	7.5	7.5	2.5
1:1	5.0	5.0	8.0	2.0
3:1	7.5	2.5	8.5	1.5
5:1	8.3	1.7	8.7	1.3

Table 3-5: Preparation of malonate buffer solutions (first ionisation) (pH range 2-4)

H₂Mal/KHMal buffer ratio	H₂Mal solution (mL)	KHMal solution (mL)	KCl solution (mL)	Water (mL)
1:9	1.00	9.00	9.1	0.9
1:7	1.25	8.75	9.1	0.9
1:5	1.67	8.33	9.2	0.8
1:3	2.50	7.50	9.3	0.7
1:1	5.00	5.00	9.5	0.5
3:1	7.50	2.50	9.8	0.2

3.5.3 Kinetic studies to establish pH-rate profile of acid-amide 9

Imide **10** (5 mg) was dissolved in THF (1 mL) and the resulting solution was dripped slowly into a KOH solution (5 mL, 0.1 mol L⁻¹). The resulting ionised acid-amide **9** formed from **10** was then used for the kinetic analysis which was conducted on a Hewlett Packard Agilent 8453 UV/Vis spectrophotometer.

The reaction was started by adding the acid-amide (50 µL) to the 1:5 carbonate buffer solution (2.5 mL) which had been left in the cell block to temperature-equilibrate for 15 minutes, and the absorbance values were recorded at pre-set time intervals (14 seconds) and integration time (0.5 seconds). The run time of the instrument was pre-set at 40,000 seconds so as to incorporate at least 10 half-lives of the hydrolysis reaction.

The pH of the cell solution was measured after the reaction was completed. The experiment was repeated using the other carbonate buffer solutions, as well as phosphate and malonate buffer solutions at different ratios, while the time interval and wavelength were kept constant.

The analysis was carried out using the Agilent Chemstation software. The first order kinetics method option in this software plots an exponential graph according to the following equation:

$$a + be^{(-kt)}$$

From this equation, the k_{obs} values and their standard deviations were calculated directly with a best fit curve fitted to data plotted as absorbance versus time.

The absorbance data at 247 nm (λ_{max} of acid-amide) were routinely used to calculate the rate constants. An example of a typical spectrum obtained by this software is shown in Appendix E.

Even though the reaction was left to run for 40,000 seconds, the infinity data were not used because of over-emphasis on the small absorbance values at the late stages of the reaction in the curve fitting, but the analyses were conducted so that stable infinity values could be seen to ensure there was no any problem of drift calculated by the software.

A graph of k_{obs} against pH was then plotted to establish the pH-rate profile of acid-amide **9** (refer to Figure 2-14).

To establish that the neutral acid-amide gave only hydrolysis products not imide, a one-off reaction in malonate buffer at pH 3.9 was carried out and subsequently, the pH was raised to 11.1 with added K_3PO_4 . The absence of any detectable absorbance change at 247 nm showed the absence of any imide in product solution.

3.5.4 Buffer dilutions

Buffer solutions were normally prepared at the concentration of 0.100 mol L^{-1} . However, at a high concentration like this exists a potential buffer catalytic problem on the rates of the hydrolysis reaction.

Buffer catalysis is known to occur for a few aryl amines with neighbouring carboxylate groups as reported by Kluger and Lam³⁸. Therefore, a study was conducted to check for any existence of buffer catalytic effect on the reactions.

The buffer dilution analysis was carried out by diluting, two-fold and four-fold, the 1:1 buffer solution of the carbonate, phosphate and malonate buffer solutions. Subsequently, the solutions were analysed by running the amide hydrolysis reactions in them while keeping all the other parameters the same. If no buffer catalysis was occurring, there would be no change in solution pH and rate of hydrolysis reaction even though the concentration of buffer solution was being halved or quartered. On the other hand, if buffer catalysis was occurring, the reaction rate would be less than that determined from the reaction run in buffer solution of 0.100 mol L⁻¹.

It was found that all the buffer solutions do not show any significant buffer catalytic reactions as the resulting reaction rates were consistent, to a measurable extent at least, with those determined for the solutions with full buffer concentration.

4 Summary and Conclusions

The initial goal of the current study was to synthesise an *endo*-acid-amide in its un-ionised form, purify it, and to obtain a full pH-rate profile for its cyclisation to release amine and anhydride.

This was initially attempted by using *N*-methylaniline but this was not successful probably due to the nature of the sterically crowded secondary amine molecule.

The synthetic plan was diverted to replace *N*-methylaniline with *p*-methoxyaniline, a less sterically crowded primary amine molecule. Again, this did not succeed as a pure acid-amide product could not be obtained. As a result, an *endo*-imide **10** was prepared, purified, and the imide was ring was opened in KOH solution to give a solution of pure acid-amide carboxylate **9** (Figure 4-1), which could then be used for kinetic analyses.

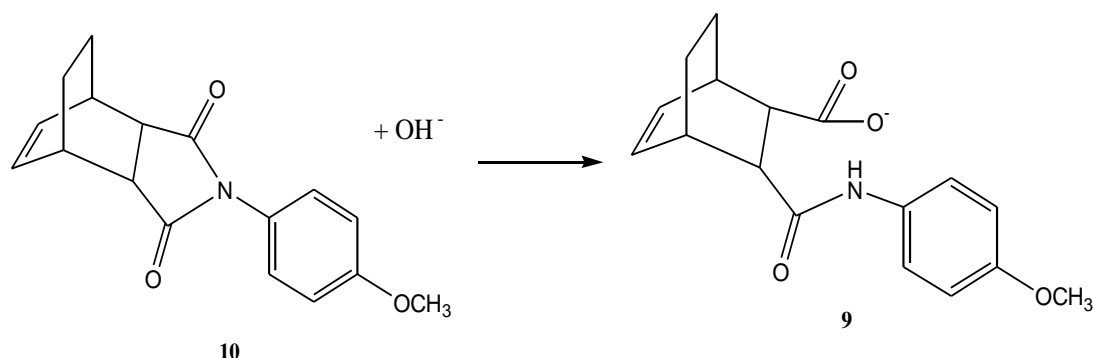


Figure 4-1: Conversion of imide to acid-amide

The pH-rate profile of acid-amide **9** was established over the pH range of 3-10. At 30°C, the limiting rate constant for hydrolysis of acid-amide **9** in its fully neutral form was calculated to be $0.44 \pm 0.03 \text{ min}^{-1}$, whereas the dissociation constant $\text{p}K_a$ was determined to be 5.1 ± 0.4 . The rate constant for formation of imide **10** from fully ionised **9**, which was represented by higher pH plateau rate (pH above 8), k_{low} , was calculated to be 0.067 min^{-1} . The neutral form of **9** was shown to undergo hydrolysis only as a product solution showed no ring opening reaction of imide when the pH was raised to 11.

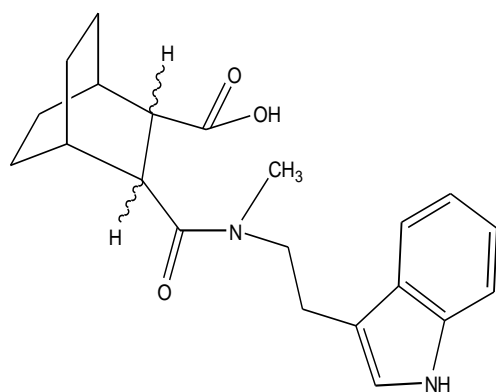


Figure 4-2: Glösenkamp's acid-amide

Although Glösenkamp's acid-amide (Figure 4-2) showed a considerably higher hydrolysis rate constant of 6.93 min^{-1} (determined at 37°C and 0.15 molL^{-1} salt concentration)²², the rate of hydrolysis of acid-amide **9** in the current study is comparable to that of Kluger's acid-amide (Figure 4-3) which has a hydrolysis rate constant of 0.87 min^{-1} (determined at 50°C)³⁴.

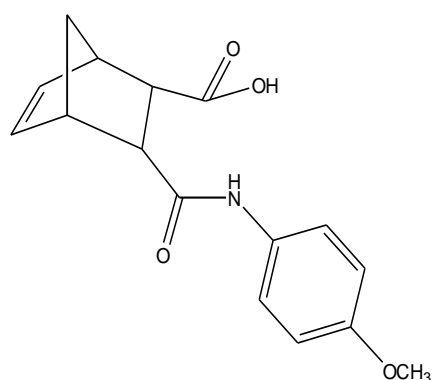


Figure 4-3: Kluger's acid-amide

In relation to prodrug application, the k_{obs} value was determined to be 0.11 min^{-1} at pH 6.02 and 0.07 min^{-1} at pH 7.06. The rate difference was not as favourably large as hoped because the pK_a was lower than anticipated from the value for similar amides in the Glösenkamp series. Although it could be concluded that the results have attained the initial aim of releasing the amine at higher rate at pH 6 than in pH 7, the difference is such that it is questionable whether there would be a potential for attaching a cytotoxic amine in place of *p*-methoxyaniline and testing the anticancer activity on cancer cells.

At higher pH where there is no neutral acid-amide, the equilibrium reaction between imide and the acid-amide carboxylate was also studied. The second order rate constant for the formation from imide and OH^- of amide carboxylate (k_f) was determined to be $74 \pm 16 \text{ L mol}^{-1} \text{ min}^{-1}$, the reverse rate constant for imide formation 0.067 min^{-1} and thereby the equilibrium constant K as 1100 L mol^{-1} .

References

1. *The human body book: An illustrated guide to its structure, function and disorders*. Dorling Kindersley Publishing, Inc: 2009.
2. World Health Organisation, World Cancer Day: Global action to avert 8 million cancer-related deaths by 2015. 3 February 2006, 2006.
3. Frank, R. C., *Fighting cancer with knowledge & hope: a guide for patients, families and health care providers*. Blank Inc, : Melbourne, Victoria, 2009.
4. Lewis, M.; Lewis, G., *Cancer: a threat to your life? or a chance to take control of your future?* Second ed.; Lewis Publications: Auckland, 2006.
5. Frei, E.; Teicher, B. A.; Holden, S. A.; Cathcart, K. N. S.; Wang, Y., Preclinical studies and clinical correlation of the effect of alkylating dose. *Cancer Research* **1988**, 48, 6417-6423.
6. Denny, W. A., Prodrug strategies in cancer therapy. *European Journal of Medicinal Chemistry* **2001**, 36, 577-595.
7. Rautio, J.; Kumpulainen, H.; Heimbach, T.; Oliyai, R.; Oh, D.; Järvinen, T.; Savolainen, J., Prodrugs: design and clinical applications. *Nature Reviews Drug Discovery* **2008**, 7, (3), 255-270.
8. Sinhababu, A. K.; Thakker, D. R., Prodrugs of anticancer agents. *Advanced Drug Delivery Reviews* **1996**, 19, 241-273.
9. Tannock, I. F.; Rotin, D., Acid pH in tumours and its potential for therapeutic exploitation. *Cancer Research* **1989**, 49, 4373-4384.
10. Warburg, O. H.; Dickens, F., The metabolism of tumours. *The American Journal of the Medical Sciences* **1931**, 182, (1), 123.

11. Weinhouse, S.; Warburg, O.; Burk, D.; Schade, A. L., On respiratory impairment in cancer cells. *Science* **1956**, 124, (3215), 267-272.
12. Prescott, D. M.; Charles, H. C.; Poulson, J. M.; Page, R. L.; Thrall, D. E.; Vujaskovic, Z.; Dewhirst, M. W., The relationship between intracellular and extracellular pH in spontaneous canine tumours. *Clinical Cancer Research* **2000**, 6, 2501-2505.
13. Vaupel, P.; Kallinowski, F.; Okunieff, P., Blood flow, oxygen and nutrient supply, and metabolic microenvironment of human tumours: a review. *Cancer Research* **1989**, 49, 6449-6465.
14. Iessi, E.; Marino, M. L.; Lozupone, F.; Fais, S.; De Milito, A., Tumour acidity and malignancy: novel aspects in the design of anti-tumour therapy. *Cancer Therapy* **2008**, 6, 55-66.
15. Newell, K.; Franchi, A.; Pouyssegur, J.; Tannock, I. F., Studies with glycolysis-deficient cells suggest that production of lactic acid is not the only cause of tumour acidity. *Proc. Natl. Acad. Sci. USA* **1993**, 90, 1127-1131.
16. Wike-Hooley, J. L.; Haveman, J.; Reinhold, H. S., The relevance of tumour pH to the treatment of malignant disease. *Radiother. Oncol.* **1984**, 2, (4), 343-366.
17. Vaupel, P. W.; Frinak, S.; Bicher, H. I., Heterogeneous oxygen partial pressure and pH distribution in C3H mouse mammary adenocarcinoma. *Cancer Research* **1981**, 41, 2008-2013.
18. Kahne, D.; Still, W. C., Hydrolysis of a peptide bond in neutral water. *Journal of the American Chemical Society* **1988**, 110, 7529-7534.
19. Bender, M. L., General acid-base catalysis in the intramolecular hydrolysis of phthalamic acid. *Journal of the American Chemical Society* **1957**, 79, 1258-1259.

20. Kirby, A. J.; Lancaster, P. W., Structure and efficiency in intramolecular and enzymic catalysis. Catalysis of amide hydrolysis by the carboxy-group of substituted maleamic acids. *Journal of the Chemical Society, Perkins Transactions 2* **1972**, (9), 1206-1214.
21. Menger, F. M.; Ladika, M., Fast hydrolysis of an aliphatic amide at neutral pH and ambient temperature. A peptidase model. *Journal of the American Chemical Society* **1988**, 110, (20), 6794-6796.
22. Glusenkamp, K.-H.; Mengede, C.; Drosdziok, W.; Jahde, E.; Rajewsky, M. F., Rapid hydrolysis of amides under physiological conditions: influence of the microenvironment on the stability of the amide bond. *Bioorganic and Medicinal Chemistry Letters* **1998**, 8, 285-288.
23. Brown, J.; Su, S. C. K.; Shafer, J. A., The hydrolysis and cyclisation of some phthalamic acid derivatives. *Journal of the American Chemical Society* **1966**, 88, (19), 4468-4474.
24. Teng, R. *pH-Sensitive anticancer prodrugs*; The University of Waikato: Hamilton, New Zealand, October, 2007.
25. Leont'eva, S. V.; Manulik, O. S.; Evstigneeva, E. M.; Bobkova, E. N.; Flid, V. R., Unconventional catalytic allylation of 5-norbornene-2,3-dicarboxylic anhydrides: 7-oxa and 7-aza analogues. *Kinetics and Catalysis* **2006**, 47, (3), 384-388.
26. Song, C. E.; Roh, E. J.; Lee, S.-g.; Shim, W. H.; Choi, J. H., Ionic liquids as powerful media in scandium triflate catalysed Diels-Alder reactions: significant rate acceleration, selectivity improvement and easy recycling of catalyst. *Chemical Communications (Cambridge, United Kingdom)* **2001**, 12, 1122-1123.
27. Kobayashi, S.; Tsuchiya, T.; Komoto, I.; Matsuo, J.-i., Scandium perfluoroalkanesulfonate-catalysed Diels-Alder reactions in an organic solvent. *Journal of Organometallic Chemistry* **2001**, 624, (1-2), 392-394.

28. Birney, D.; Lim, T. K.; Koh, J. H. P.; Pool, B. R.; White, J. M., Structural investigations into the *retro*-Diels-Alder reaction. Experimental and theoretical studies. *Journal of the American Chemical Society* **2002**, 124, (18), 5091-5099.
29. McMurry, J., Conjugated dienes and ultraviolet spectroscopy. In *Organic Chemistry*, 6th ed.; Kiselica, S., Ed. Cornell University: 2004.
30. Curran, T. P.; Borysenko, C. W.; Abelleira, S. M.; Messier, R. J., Intramolecular acylolysis of amide derivatives of Kemp's triacid: strain effects and reaction rates. *Journal Of Organic Chemistry* **1994**, 59, 3522-3529.
31. Billett, N. G.; Phillis, A. T.; Main, L.; Nicholson, B. K.; Denny, W. A.; Hay, M. P., The 3-*N*-phenyl amide of *all-cis*-cyclopentane-1,2,3,4-tetracarboxylic acid as a potential pH-sensitive amine-releasing prodrug; intervention of imide formation around neutral pH. *ARKIVOC* **2006**, iii, 183-201.
32. Jencks, W. P., Practical kinetics. In *Catalysis in chemistry and enzymology*, Dover Publications, Inc.: New York, 1968; pp 555-565.
33. Kluger, R.; Chin, J.; Choy, W.-W., Carboxylic acid participation in amide hydrolysis. Reactivity of intermediates in the internally catalysed hydrolysis of *N*-substituted 2,3-dimethylmaleamic acids. *Journal of the American Chemical Society* **1979**, 101, (23), 6976-6980.
34. Kluger, R.; Lam, C.-H., Carboxylic acid participation in amide hydrolysis. External general base catalysis and general acid catalysis in reactions of norbornenylanilic acids. *Journal of the American Chemical Society* **1978**, 100, (7), 2191-2197.
35. Diels, O.; Alder, K., Synthesen in der hydroaromatischen Reihe. *Justus Liebig's Annalen der Chemie* **1928**, 460, 98-122.

36. Weast, R. C., *CRC Handbook of Chemistry and Physics*. 62nd ed.; Boca Raton, FL: CRC Press: 1981.
37. *CRC Handbook of Chemistry and Physics*. 84th ed.; CRC Press,; Cleveland, Ohio, 2003/2004.
38. Kluger, R.; Lam, C.-H., The effects of leaving group basicity on the hydrolysis of aryl-substituted maleanilinic acids. *Journal of the American Chemical Society* **1975**, 97, (19), 5536-5540.
39. Guggenheim, E. A., *Philosophical Magazine* 1926, p 538.
40. Moore, J. W.; Pearson, R. G., *Kinetics and Mechanism*. Third ed.; John Wiley & Sons, Inc.: 1981.

Appendix A – Glycolytic pathway

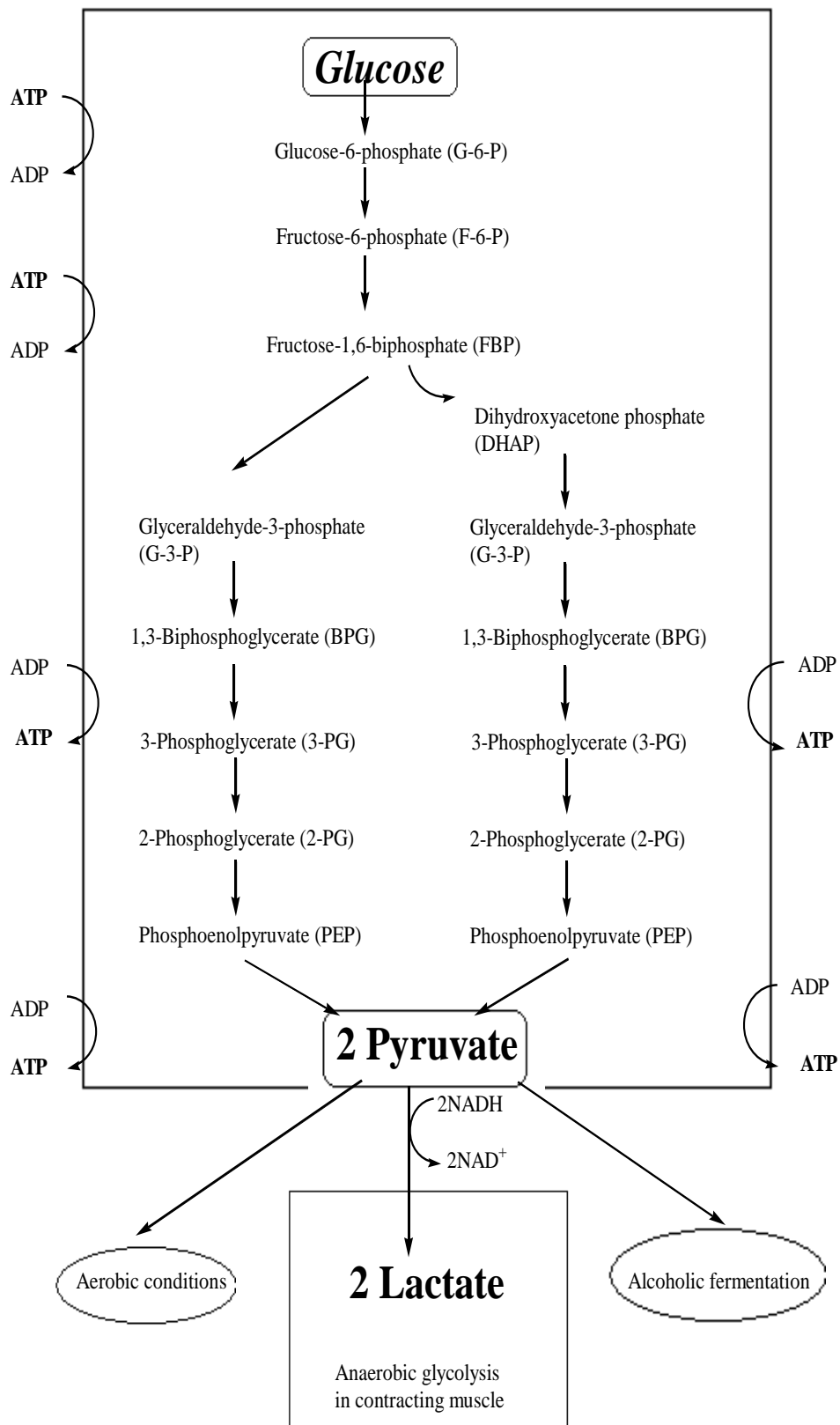


Figure A-1: Glycolytic pathway

Appendix B - ¹H NMR spectrum of imide 10

99

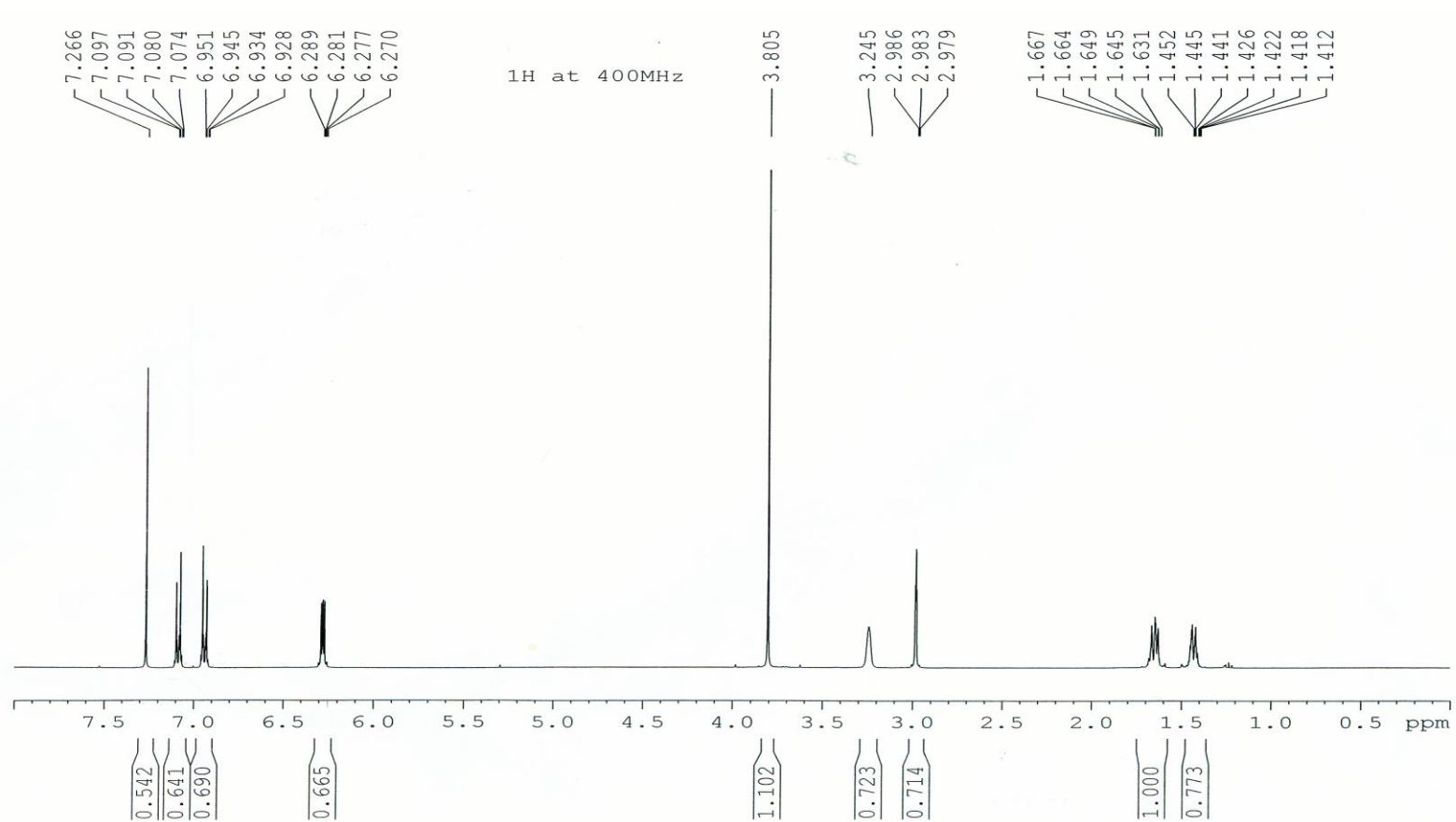
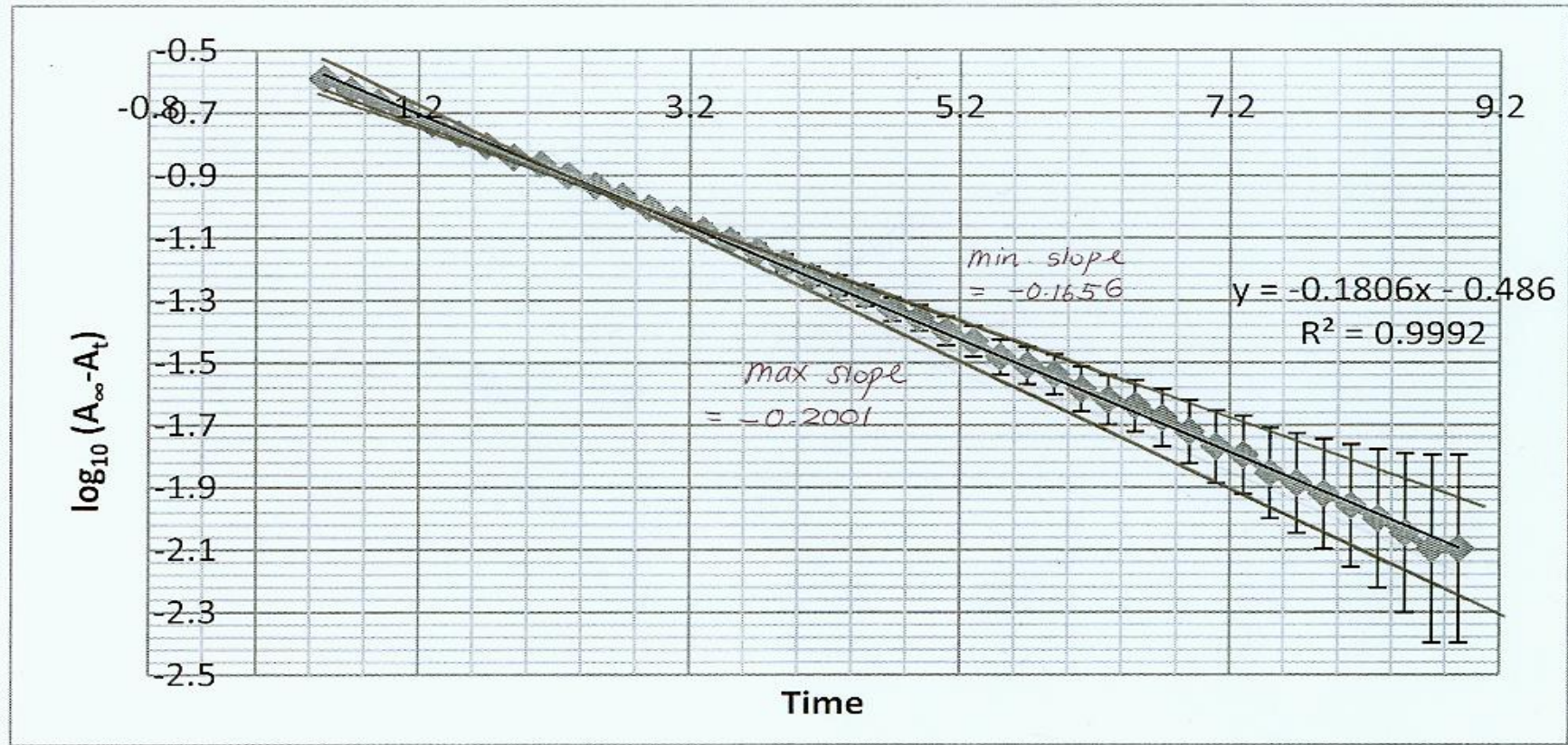


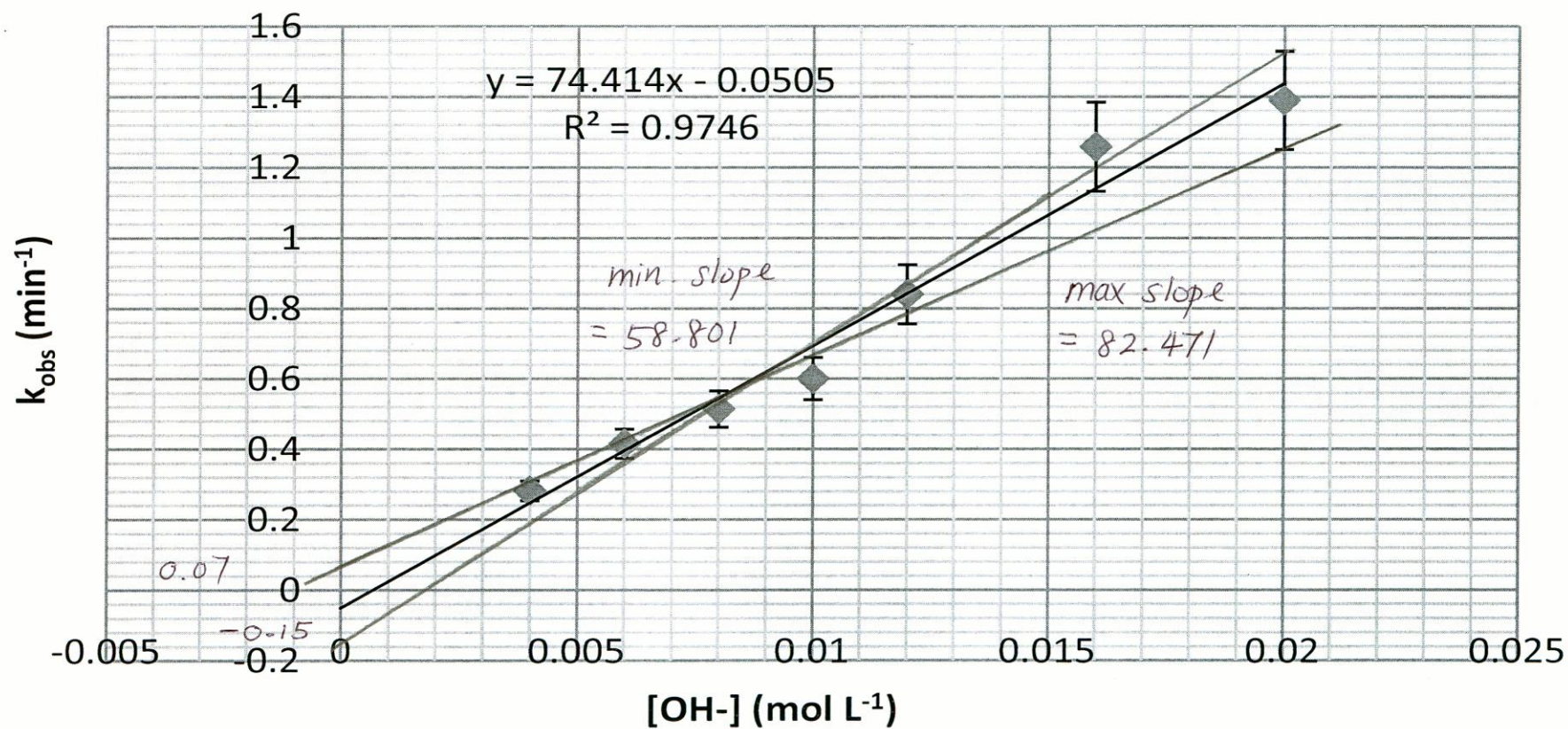
Figure B-1: Proton NMR of imide 10

Appendix C - Graph for determining errors



$$\text{Slope} = -0.1806 \pm 0.0195$$
$$= -0.1806 \pm 10\% \text{ (approximate)}$$

Figure C-1: Graph for determining error of k_{obs}



$$k_f = \text{slope} = 74. \pm 16 \text{ L mol}^{-1} \text{ min}^{-1}$$

$$k_r = \text{y-intercept} = -0.05 \pm 0.12 \text{ min}^{-1}$$

Figure C-2: Graph for determining errors of k_r and k_f

Appendix D - Error estimation of k_{lim} and pK_a

69

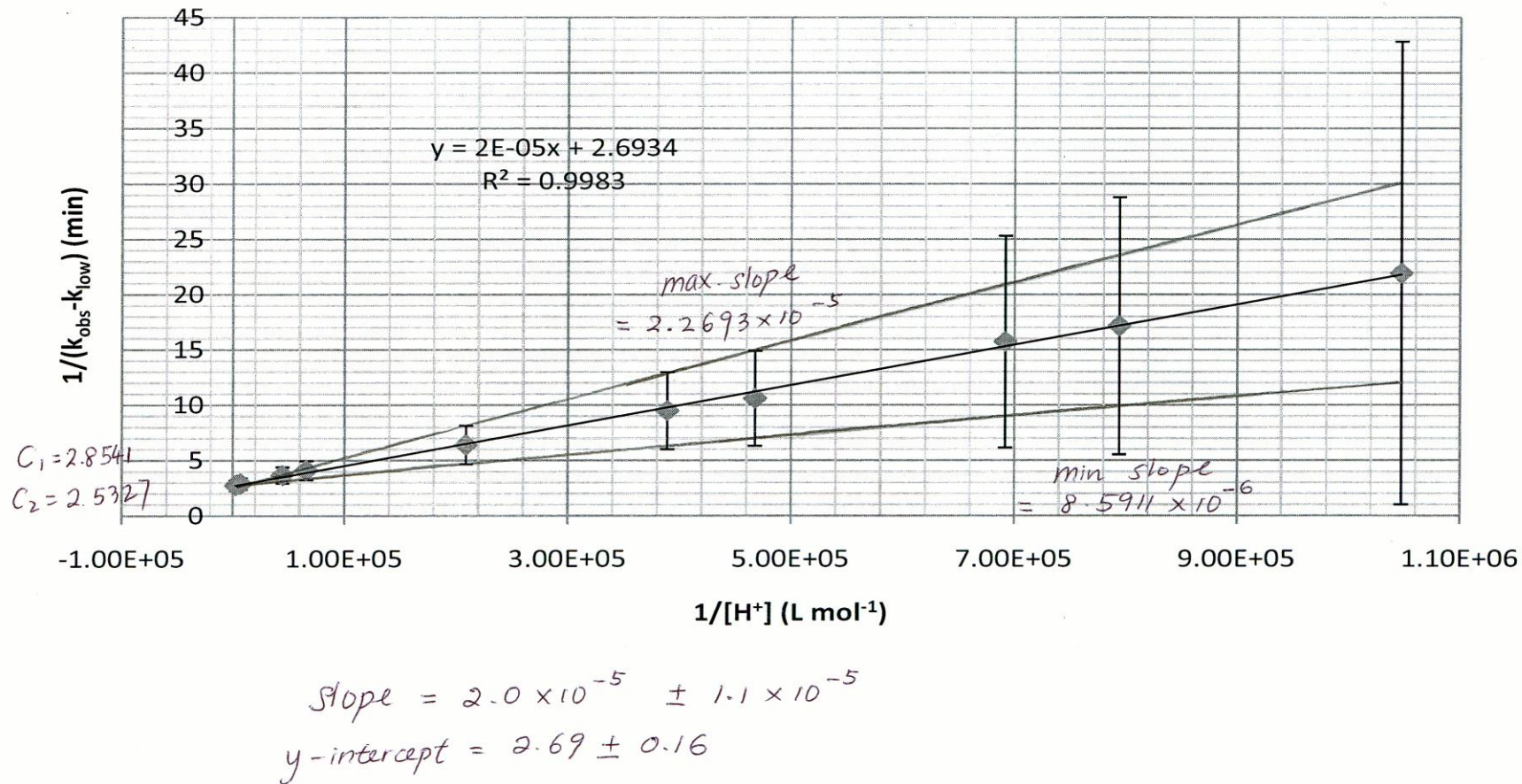


Figure D-1: Graph for determining errors of k_{lim} and pK_a

The values for slope and y-intercept were calculated to be $2.0E+05 \pm 1.1E+05$ and 2.69 ± 0.16 . These were calculated from the maximum and minimum slopes and y-intercepts of the following graph.

Error estimation of pK_a

From equation (7):

$$K_a = \frac{\text{slope}}{\text{y-intercept}} = 7.4256E - 06$$

Therefore,

$$\frac{\sigma_{K_a}}{K_a} = \sqrt{\left(\frac{\sigma_{\text{slope}}}{\text{slope}}\right)^2 + \left(\frac{\sigma_{\text{y-intercept}}}{\text{y-intercept}}\right)^2}$$

$$\frac{\sigma_{K_a}}{7.4256E-06} = \sqrt{\left(\frac{1.1E-05}{2.0E-05}\right)^2 + \left(\frac{0.16}{2.69}\right)^2}$$

$$\sigma_{K_a} = 4.1079E - 06$$

$$\text{Since } pK_a = -\log_{10} K_a = 5.129$$

$$\therefore \sigma_{pK_a} = 0.3499$$

Therefore, $pK_a = 5.13 \pm 0.35$

Error estimation of k_{lim}

From equation (7):

$$\frac{1}{(k_{lim} - k_{low})} = \text{y-intercept}$$

$$k_{lim} = \frac{1}{y\text{-intercept}} + k_{low} = 0.4383$$

$$\sigma_{k_{lim}} = \sigma_{\left(\frac{1}{y\text{-intercept}}\right)} + \sigma_{k_{low}} = 0.0319$$

Therefore, $k_{lim} = 0.044 \pm 0.032$

Appendix E - UV/Vis spectra obtained from Agilent Chemstation Software

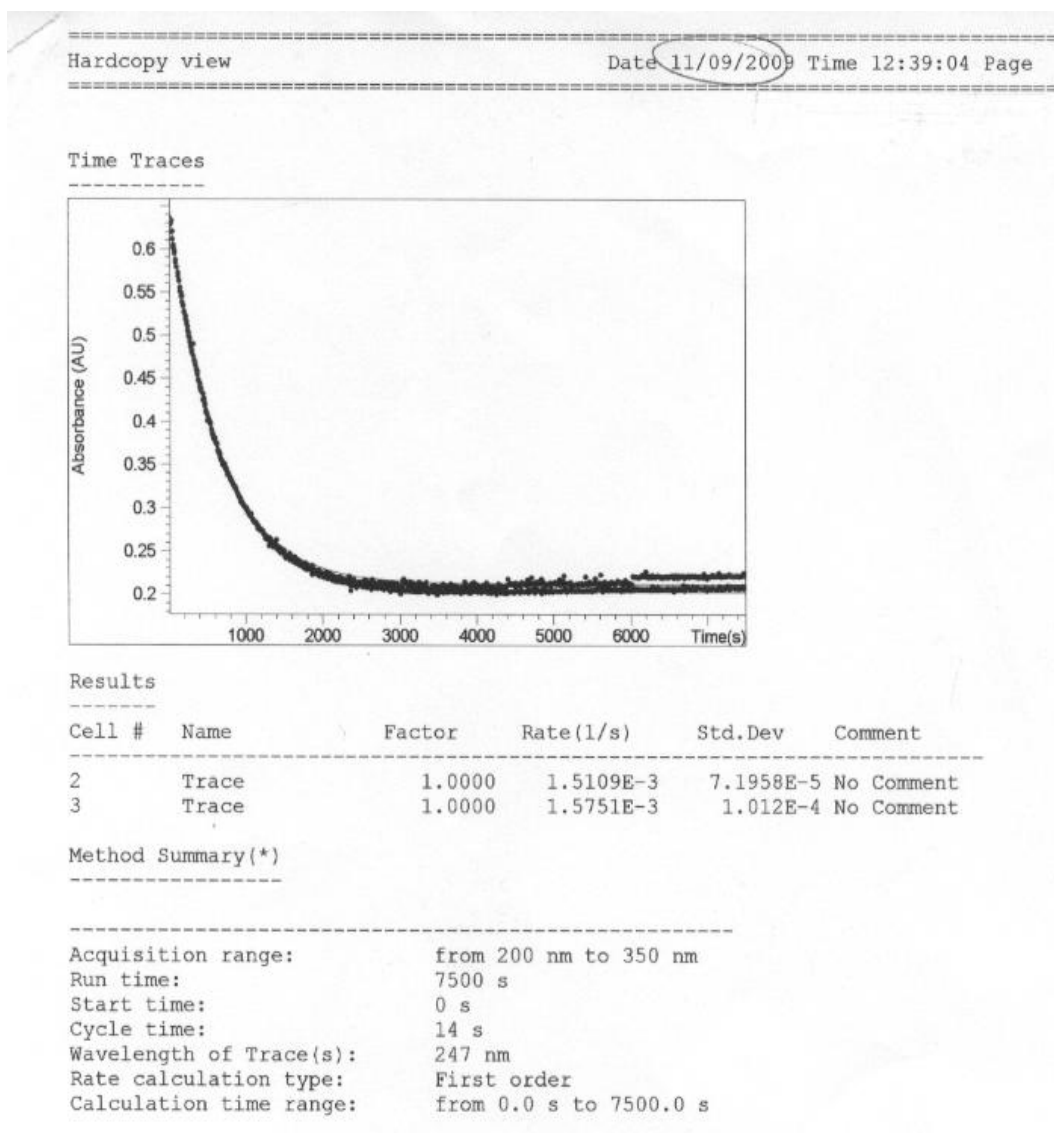
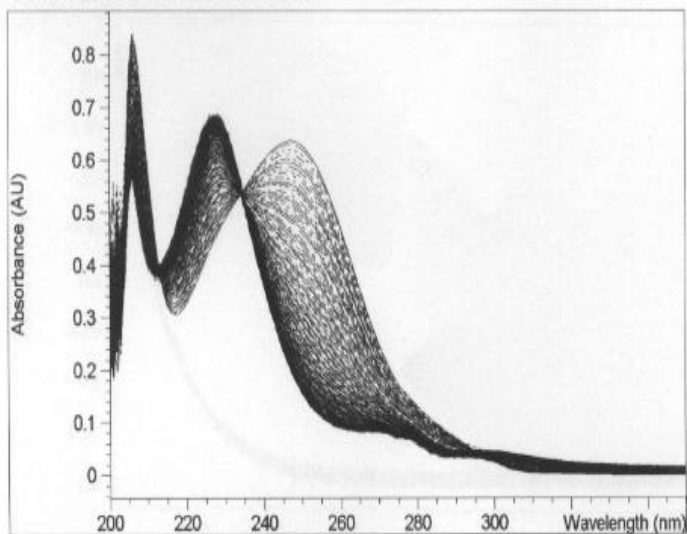


Figure E-1: Example of the kinetic analysis data

Sample Spectra of Cell 2



Sample Spectra of Cell 3

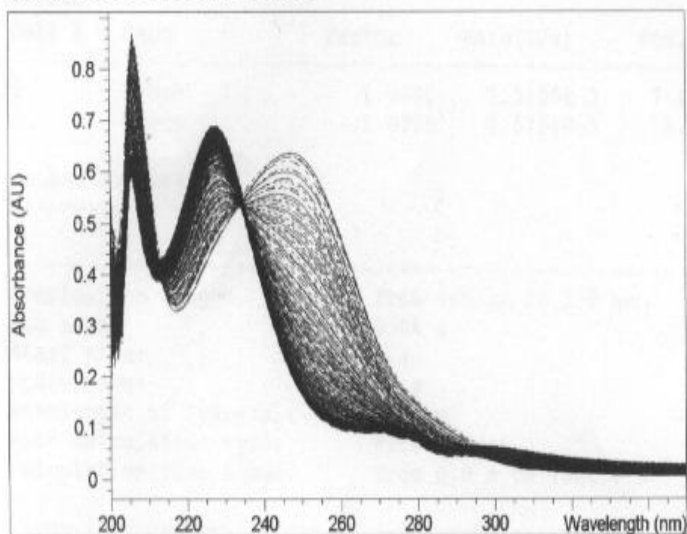


Figure E-2: Typical repetitive scanning spectra for hydrolysis of acid-amide

Appendix F – Theory of first order rate constants³²

The rate of a first-order reaction is proportional to the concentration of a single species:



Other reactants can be present but will be zero-order. A first order reaction is described by a rate constant, k , with the dimensions of reciprocal time, such as sec^{-1} or min^{-1} :

$$\text{Rate} = v = -\frac{d[A]}{dt} = \frac{d[P]}{dt} = k [A] \quad \text{----- (2)}$$

Equation 2 for a first-order reaction may be integrated from t_0 to the time of an experimental measurement according to the following equations, in which A_0 is the concentration of A at zero time.

$$\int_{A_0}^A \left(-\frac{d[A]}{dt}\right) = k \int_{t_0}^t dt$$

$$-\ln[A] + \ln[A]_0 = kt$$

$$\ln \frac{[A_0]}{[A]} = kt$$

$$-\ln[A] + \ln[A_0] = kt$$

$$-\log_{10}[A] + \log_{10}[A_0] = \frac{k}{2.303} t$$

$$\log_{10}[A] = \log_{10}[A_0] - \frac{k}{2.303} t \quad \text{----- (3)}$$

The variables in these equations are $[A]$ and t , so that the concentration of A decreases exponentially and a plot of $\log_{10} [A]$ against t is linear with a slope of $-k/2.303$. The half-life, $t_{1/2}$, of the reaction is the time at which the concentration of A has decreased to half of its initial value, $0.5 A_0$:

$$kt_{1/2} = \ln \frac{A_0}{0.5A_0} = \ln 2 = 0.693 \quad \text{----- (4)}$$

When working with a UV/Vis spectrophotometer, absorbance, A increases with time if the product absorbs more than the reactant at the monitoring wavelength. In this case, $A_\infty - A_0$ is thus directly proportional to $[A_0]$, and $A_\infty - A_t$ is directly proportional to $[A_t]$. Therefore, by plotting $\log_{10}[A_\infty - A_t]$ against t the rate constant k can be calculated from the slope of the straight line:

$$k = -\text{slope} \times 2.303 \quad \text{----- (5)}$$

And therefore $t_{1/2}$ can be calculated from equation 4:

$$\therefore t_{1/2} = \frac{0.693}{k} \quad \text{----- (5)}$$

In practice, if absorbance increases during an experiment, $\log_{10}(A_\infty - A_t)$ can be plotted against time. If absorbance is decreasing, then $\log_{10}(A_t - A_\infty)$ is plotted against t .

An alternative method to determine the reaction rate constant for a first-order reaction is the Guggenheim method^{39, 40}. This method is used when the final absorbance reading A_∞ is unreliable or is taking too long to achieve.

According to Guggenheim, if times t_1, t_2, t_3 , etc., and $t_1 + \Delta t, t_2 + \Delta t, t_3 + \Delta t$, etc., are selected (where Δt is a constant time increment), then the graph of $\log_{10}[A_t - (A_{t+\Delta t})]$ against t or $[\log_{10}(A_{t+\Delta t}) - A_t]$ against t can be plotted to obtain a linear plot, the slope of which is used to determine the rate constant k as in equation 5.

To be able to use the Guggenheim method, it must be certain that the reaction is a simple first-order reaction, since other more complex reactions (e.g. reversible and concurrent first-order reactions) can give

apparent linearity and false rate constants by this method. On the other hand, the time interval Δt should best be two or three times as great as the half life period of the reaction, for accuracy purposes.